The current issue and full text archive of this journal is available at
www.emeraldinsight.com/0961-5539.htm

Geometry effects on conjugate natural convection heat transfer in vertical eccentric annuli

Maged A.I. El-Shaarawi, Esmail M.A. Mokheimer and Ahmad Jamal
Mechanical Engineering Department, King Fahd University of Petroleum and Minerals, Dhahran, Saudi Arabia

Received 4 February 2006
Revised 29 March 2006
Accepted 12 June 2006

Abstract

Purpose – To explore the effect of the annulus geometrical parameters on the induced flow rate and the heat transfer under the conjugate (combined conduction and free convection) thermal boundary conditions with one cylinder heated isothermally while the other cylinder is kept at the inlet fluid temperature.

Design/methodology/approach – A finite-difference algorithm has been developed to solve the bipolar boundary-layer equations for the conjugate laminar free convection heat transfer in vertical eccentric annuli.

Findings – Numerical results are presented for a fluid of Prandtl number, $Pr = 0.7$ in eccentric annuli. The geometry parameters of NR_2 and E (the fluid-annulus radius ratio and the eccentricity, respectively) have considerable effects on the results.

Practical implications – Applications of the obtained results can be of value in the heat-exchanger industry, in cooling of underground electric cables, and in cooling small vertical electric motors and generators.

Originality/value – The paper presents results that are not available in the literature for the problem of conjugate laminar free convection in open-ended vertical eccentric annular channels. Geometry effects having been investigated by considering fluid annuli having radii ratios $NR_2 = 0.1$ and 0.3, 0.5 and 0.7 and four values of the eccentricity $E = 0.1$, 0.3, 0.5 and 0.7. Moreover, practical ranges of the solid-fluid conductivity ratio (KR) and the wall thicknesses that are commonly available in pipe standards have been investigated. Such results are very much needed for design purposes of heat transfer equipment.

Keywords Convection, Channel flow, Numerical analysis

Paper type Research paper

Nomenclature

a = Location of the positive pole of the bipolar coordinate system on the x-axis of the Cartesian coordinate system (constant in the bipolar transformation equations, equal to $r_i \sinh \eta_i$ or $r_o \sinh \eta_o$), m

A = Cross-sectional area of the channel, $\pi(r_{io}^2 - r_{oi}^2)$

a^* = Heat transfer coefficient, $q''/(T_w - T_m)$

c_p = Specific heat of fluid at constant pressure, kJ/kg K

D_h = Hydraulic or equivalent diameter of annulus, $2(r_{io} - r_{oi}) = 2a(1 - NR_2)$ cosech η_o, m

e = Eccentricity (distance between the axes of the two cylinders forming the eccentric annulus), a (coth η_o − coth η_i), m

E = Dimensionless eccentricity, $e/(r_{io} - r_{oi})$

F = Dimensionless volumetric flow rate, $F = U_o(1 - NR_2^2)$

International Journal of Numerical Methods for Heat & Fluid Flow
Vol. 17 No. 5, 2007
pp. 461-493

0961-5539
DOI 10.1108/09615530710752955

Gr = Grashof number, $(g\beta(T_w - T_o)D_h^3)/\gamma^2$

Gr^* = Modified Grashof number, $(GrD_h)/l$

h = Coordinate transformation scale factor, $a(\cosh \eta - \cos\xi)$

H = Dimensionless coordinate transformation scale factor, $h/D_h = (0.5\sinh(\eta_o))/((1-N)\times(\cosh(\eta) - \cos(\xi)))$

$HF_{i,ex}$ = Dimensionless local heat flux on inner interface at channel exit

$HF_{o,ex}$ = Dimensionless local heat flux on outer interface at channel exit

i = Index for bi-polar grid in the η-direction and the cylindrical grid in the radial direction

j = Index for the bi-polar grid in the ξ-direction and the cylindrical grid in the tangential direction

k_f = Thermal conductivity of fluid, W/m.K

k_s = Thermal conductivity of solid, W/m.K

KR = Solid-fluid conductivity ratio, k_s/k_f

l = Height of annulus, m

L = Dimensionless height of channel (value of Z at channel exit), $1/Gr^*$

M = No. of intervals in each of the ξ and ϕ directions

N = Number of intervals in the η-direction

NR_1 = Ratio between inner radius of inner cylinder and inner radius of outer cylinder, r_{ii}/r_{io}

NR_2 = Ratio between outer radius of inner cylinder and inner radius of outer cylinder (Fluid annulus radius ratio), r_{oi}/r_{io}

NR_3 = Dimensionless inner radius of outer cylinder, $r_{io}/r_{io} = 1$

NR_4 = Ratio between outer radius of outer cylinder and inner radius of outer cylinder, r_{oo}/r_{io}

NSI = No. of radial intervals in the inner cylinder wall

NSO = No. of radial intervals in the outer cylinder wall

Nu_i = Local Nusselt number at any point on the inner wall, $a_i^* D_h/k$

Nu_o = Local Nusselt number at any point on the outer wall, $a_o^* D_h/k$

$\overline{Nu_i}$ = Nusselt number averaged around the periphery of the inner wall, $\frac{2(1-N)}{N\pi}\int_0^{\pi} Nu_i H(\eta_i, \xi)d\xi$

$\overline{Nu_o}$ = Nusselt number averaged around the periphery of the outer wall, $\frac{2(1-N)}{\pi}\int_0^{\pi} Nu_o H(\eta_o, \xi)d\xi$

$Nu_{i,ex}$ = Nusselt number on inner interface at channel exit

$Nu_{o,ex}$ = Nusselt number on outer interface at channel exit

$\overline{Nu}_{i,e}$ = Average Nusselt number on inner solid-fluid interface at the channel exit

$\overline{Nu}_{o,e}$ = Average Nusselt number on outer solid-fluid interface at the channel exit

p = Pressure of fluid inside the channel at any cross-section, N/m^2

P = Dimensionless Pressure defect of fluid inside the channel at any cross section, $\frac{P' D_h^4}{\rho l^2 \gamma^2 Gr^{*2}}$

p_s = Hydrostatic pressure, ρgz, N/m^2

P' = Pressure defect at any point, $p - p_s$, N/m^2

q'' = local heat flux at either boundary of the annulus defined to be positive when it heats the fluid, $-k\partial T/\partial n^* = \pm(k/h)(\partial T/\partial \eta)$ where the upper and lower signs stand for the inner and outer walls, respectively, in case of fluid heating and vice versa in case of fluid cooling

q = heat gained or lost by fluid from the entrance up to a particular elevation in the annulus, $\rho_o f c_p (T_m - T_o)$

$\bar{q}$ = heat gained or lost by fluid from the entrance up to the annulus exit, i.e. value of q at $z = l$, $\rho_o f c_p(\bar{T}_m - T_o)$

$\bar{Q}$ = Dimensionless heat absorbed up to the annulus exit, i.e. values of Q at $z = l$, $F\theta_{m,ex}$

r_{ii} = Inner radius of inner cylinder, m

r_{oi} = Outer radius of inner cylinder, m

r_{io} = Inner radius of outer cylinder, m

r_{oo} = Outer radius of outer cylinder, m

R = Dimensionless radial coordinate, r/r_{io}

ΔR_i = $(NR_2 - NR_1)/NSI$

ΔR_o = $(NR_4 - NR_3)/NSO$

T_o = Ambient or fluid entrance temperature, K

T_w = Isothermal temperature of heated wall, K

u = Axial (stream wise) velocity component, m/s

u_o = Entrance axial velocity, $\bar{u}$

$\bar{u}$ = Average axial velocity (volume flow rate per unit area), $\int_A u\,dA/A$

U = Dimensionless axial velocity at any point, $(ur_{io}^2)/l\gamma Gr*$

U_o = Dimensionless axial velocity at annulus entrance, $(u_o r_{io}^2)/l\gamma Gr*$

v = η-velocity component, m/s

V = Velocity vector or dimensionless η-velocity component, $\nu D_h/\gamma$

w = ξ-velocity component, m/s

W = Dimensionless ξ-velocity component, wD_h/γ

x = The first transverse direction in the Cartesian coordinate system, $x = (a\sinh(\eta))/(\cosh(\eta) - \cos(\xi))$

X = Dimensionless value of x, x/r_{io}

X_f = Dimensionless x-coordinate of the fluid annulus

X_{si} = Dimensionless x-coordinate of the inner cylinder wall

X_{so} = Dimensionless x-coordinate of the outer cylinder wall

z = Axial coordinate in both the Cartesian and bipolar coordinate systems, m

Z = Dimensionless axial coordinate in both the Cartesian and bipolar coordinate systems, z/lGr^*

ΔZ = Dimensionless Axial step increment, $\Delta z/lGr^*$

Greek letters

β = Volumetric coefficient of thermal expansion, K^{-1}

δ_i = Dimensionless thickness of inner cylinder wall, $NR_2 - NR_1$

δ_o = Dimensionless thickness of outer cylinder wall, $NR_4 - NR_3$

η = First transverse bi-polar coordinate

η_i = Value of η on the inner interface, $\eta_i = \log_e[(NR_2(1+E^2) + (1-E^2))/(2NR_2E) + ((NR_2(1+E^2) + (1-E^2))/(2NR_2E))^2 - 1]$

η_o = Value of η on the outer interface, $\eta_o = \log_e[(NR_2(1-E^2) + (1+E^2)/(2E) + ((NR_2(1-E^2) + (1+E^2))/(2E))^2 - 1]$

$\Delta\eta$ = Numerical grid mesh size in η-direction, $(\eta_i - \eta_o)/N$

θ = Dimensionless temperature, $(T - T_o)/(T_w - T_o)$ for isothermal walls case

θ_f = Value of θ in the fluid annulus

$\theta_{m,ex}$ = Mean bulk temperature at channel exit

θ_{si} = Value of θ in the inner solid wall

θ_{so} = Value of θ in the outer solid wall

μ = Dynamic viscosity of fluid, $N.s/m^2$

γ = Kinematic viscosity of fluid, μ/ρ, m^2/sec

ρ = Density of fluid, kg/m^3

Ψ = Normalized value of ξ, ξ/π

α = Thermal diffusivity of fluid, $k/\rho c_p$, m^2/sec

ξ = Second transverse bi-polar point.

$\Delta\xi$ = Numerical grid mesh size in ξ-direction, π/M

ϕ = Angle along the cylinder walls

$\Delta\phi$ = Numerical grid mesh size in ϕ-direction, π/M

Subscripts

f = fluid

i = inner wall

fd = fully developed

o = outer wall

s = solid or static

Introduction

The study of steady laminar induced flow in vertical eccentric annuli with conjugate heat transfer is of great importance because of its many engineering applications in electrical, nuclear, solar and thermal storage fields. A typical application is that of a gas cooled nuclear reactor, in which cylindrical fissionable fuel elements are placed

axially in vertical coolant chambers within the graphite moderator; the cooling gas is flowing along the channel parallel to the fuel element. In such a system, laminar free convection may provide the sole means of the necessary cooling during the shut down or accident periods.

In conventional heat transfer analyses, it is common practice to consider the temperature or the heat flux at the fluid-wall interface as known a priori. Thus, the energy equation for the fluid alone has to be solved. The results thus obtained are good only for heat transfer in flows bounded by walls having extremely small thermal resistance, i.e. very high thermal conductivity and/or very small thickness. However, in actual practice, the wall thermal resistance is finite and the thermal conditions at the fluid-wall interface are different from their counterparts imposed at the other surface of the solid walls. Such type of problems, where heat conduction in the solid is coupled with convective heat transfer in the fluid, is often referred to as conjugate problems. If the bounding cylinder walls are thick and/or have low thermal conductivity, conjugation (coupling of conduction and convection) must be taken into account as it can significantly affect the heat transfer, otherwise it can be neglected.

Considerable work has been done to study the problem of flow and conjugate heat transfer in various geometries and annuli, both concentric and eccentric. Anand and Tree (1987) studied the effect of axial conduction in a tube wall on the steady-state laminar convective heat transfer. Kim and Anand (1990) numerically investigated the effect of wall conduction on the free convection between asymmetrically heated vertical plates with uniform wall heat flux. Kim *et al.* (1991) numerically studied laminar free convection heat transfer in channels formed between series of vertical parallel plates with an embedded line heat source in order to investigate the effect of repeated boundary condition and wall conjugation on mass flow rate, maximum surface temperature, and average surface Nusselt number. Sakakibara *et al.* (1987), analytically, investigated the steady conjugate heat transfer problem in an annulus with a heated core and an insulated outside tube when the laminar flow is hydrodynamically fully developed. El-Shaarawi *et al.* (1995) presented a finite-difference scheme to solve the transient conjugate forced convection in a concentric annulus with simultaneously developing hydrodynamic and thermal boundary layers. Using a finite-difference technique, El-Shaarawi and Negm (1999) solved the laminar conjugate natural convection problem in vertical open-ended concentric annuli.

In spite of the many studies reported in the literature for the conventional case of either forced or free convection in eccentric annuli (Shu and Wu, 2002; Redberger and Charles, 1962; Cheng and Hwang, 1968; Trombetta, 1972; Manglik and Fang, 1995; Feldman *et al.*, 1982a, b; El-Shaarawi *et al.*, 1998; El-Shaarawi and Mokheimer, 1998, 1999), a thorough literature survey revealed that there are only two works available for the conjugate case. The first is that of El-Shaarawi and Haider (2001) for the forced-convection case and the second is that of Jamal (2002) for free convection. El-Shaarawi and Haider (2001) presented forced-convection results for a fluid of Prandtl number, $Pr = 0.7$ flowing in a fluid annulus of radius ratio, $NR_2 = 0.5$ with eccentricity, $E = 0.1$, 0.3, 0.5 and 0.7. On the other hand, Jamal (2002) presented free-convection results under two different thermal boundary conditions for a fluid of $Pr = 0.7$ flowing in eccentric annuli having a wide range of geometrical parameters ($E = 0.1$, 0.3, 0.5, 0.7 and $NR_2 = 0.1$, 0.3, 0.5, 0.7) and a wide range of conjugation parameters (solid-fluid thermal conductivity ratio, KR = 1, 5, 10, 50, 100, 1,000 and

four pairs of inner and outer cylinder wall dimensionless thicknesses, δ_o and $\delta_i = 0.02$ and 0.01; 0.1 and 0.05; 0.2 and 0.1; and 0.4 and 0.2).

The present paper presents numerical results that explore the effect of the annulus geometrical parameters on the induced flow rate and the heat transfer under the conjugate (combined conduction and free convection) thermal boundary conditions with one cylinder heated isothermally while the other cylinder is kept at the inlet fluid temperature. It is worth mentioning that the conjugation, due to the presence of solid walls of finite thermal resistances, causes the free-convection results (such as the induced flow rate and the corresponding channel height) to vary from that corresponding to the conventional case.

Governing equations

Figure 1 shows the plan and the elevation of the geometry under consideration. The vertical eccentric annulus, shown in Figure 1, is of finite height, open at both ends and is immersed in a stagnant Newtonian fluid of infinite extent maintained at constant temperature T_o. Free convection flow is induced inside this annular channel as a result of heating one of the channel walls isothermally while keeping the other wall at ambient temperature. Thus, two cases are under investigation. The first case is named case (I) in which the heated wall is the inner surface of the inner cylinder whereas the other case is called case (O) in which the heated wall is the outer surface of the outer cylinder. The fluid enters the channel at the ambient temperature T_o. It is evident from Figure 1, that the eccentric annular geometry is symmetric about line AB, therefore, only half of the geometry need to be considered in the analysis. Figure 2 shows the 2-D cross-section of that half (with the numerical mesh points).

The fluid is assumed to be Newtonian. The flow is steady, laminar, enters the eccentric annulus with a uniform velocity distribution (U_o) and then the development of its hydrodynamic and thermal boundary layers occurs. Body forces in other than the vertical direction, viscous dissipation, internal heat generation and radiation heat transfer are absent. Unless the channel is sufficiently high, fully developed flow conditions cannot be achieved. The governing equations describing the flow and heat transfer through the eccentric annulus are the well known continuity, momentum and energy equations given by Hughes and Gaylord (1964) in a general orthogonal curvilinear coordinate system.

The bi-polar coordinate system has been used in this investigation to describe the flow and heat transfer in the eccentric fluid annulus. In this bipolar coordinate system, the boundary surfaces of the fluid annulus are corresponding to constant values of one of the coordinates (η) and the other coordinate (ξ) comprises another set of eccentric annuli whose centers lie on the y-axis and orthogonally intersect the boundaries of the fluid annulus. This bi-polar coordinate system is shown in Figure 3. However, since the cylinder solid walls have uniform thicknesses, the cylindrical coordinate system is more appropriate for these solid walls. Therefore, the energy equation for each of the inner and outer solid cylinder walls is expressed in cylindrical coordinates. Some parabolic-flow assumptions (El-Shaarawi and Mokheimer, 1999) will be used to simplify the governing equations. These assumptions include: the pressure is a function of the axial coordinate only ($\partial p/\partial \eta = \partial p/\partial \xi = 0$), the axial diffusions of momentum and energy are neglected ($\partial^2/\partial z^2 = 0$), and the η-velocity component (v) is much smaller than the ξ- and z-velocity components (w and u).

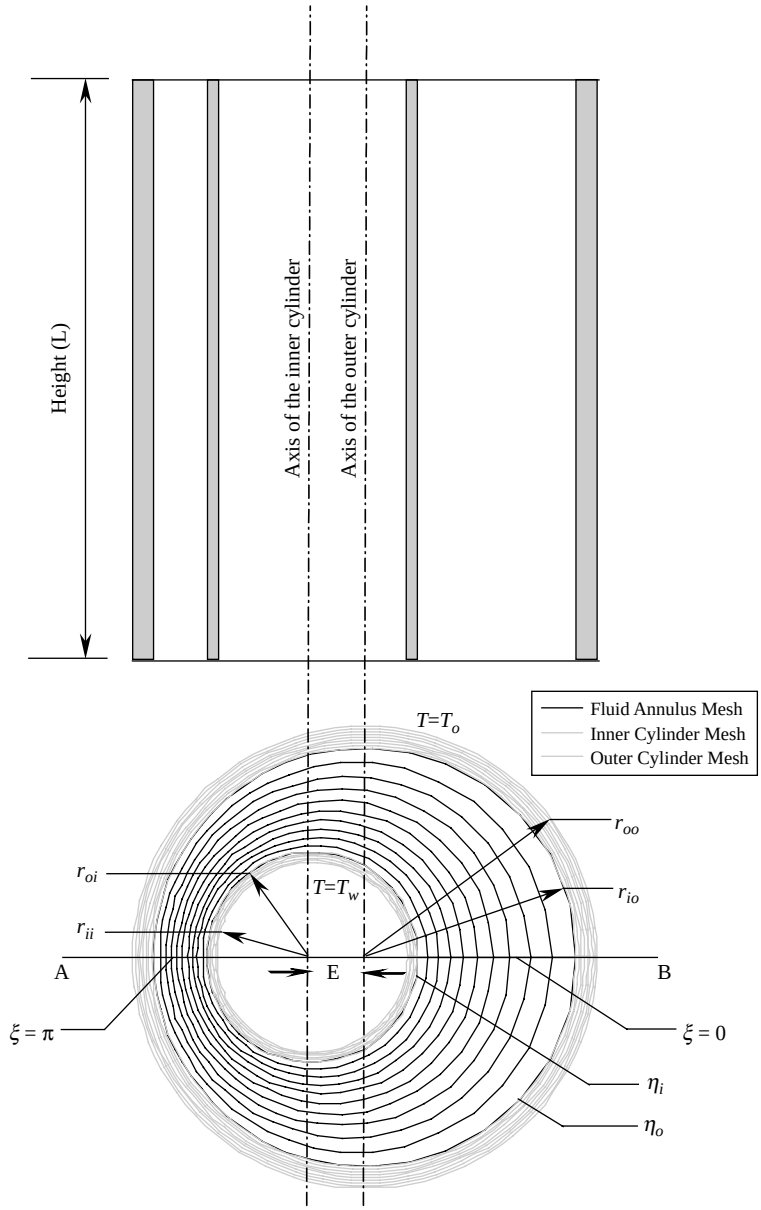

Figure 1.
Two-dimensional plan and elevation of the geometry under consideration

Introducing the dimensionless parameters given in the nomenclature, carrying out the order of magnitude analysis and taking into consideration that the latter assumption results in dropping the η-momentum equation, the governing equations can be written in the following dimensionless forms:

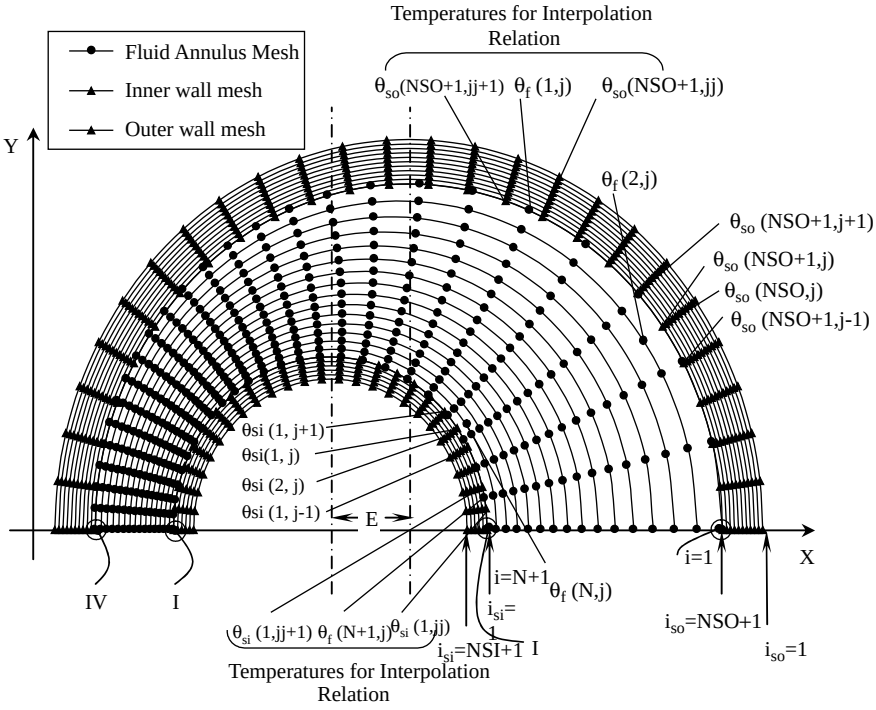

Figure 2.
Two-dimensional half symmetric mesh of eccentric annuli, $NR_2 = 0.5$, $E = 0.5$, NSO = 10, NSI = 5, $N = 15$, $M = 25$, $\delta_i = 0.05$, $\delta_o = 0.1$

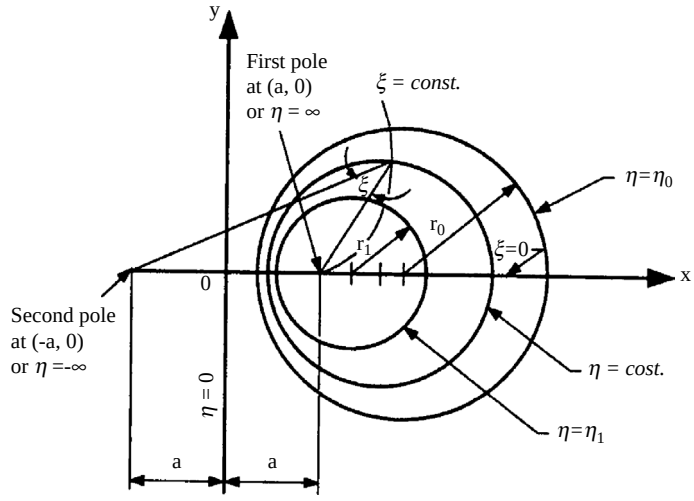

Figure 3.
Bi-polar coordinate system

- Continuity equation:

$$\frac{\partial(HW)}{\partial\xi}+\frac{\partial(HV)}{\partial\eta}+4(1-\mathrm{NR}_2)^2\frac{\partial(UH^2)}{\partial Z}=0 \tag{1}$$

- Momentum equation in Z-direction:

$$\frac{W}{H}\frac{\partial U}{\partial\xi}+\frac{V}{H}\frac{\partial U}{\partial\eta}+4(1-\mathrm{NR}_2)^2U\frac{\partial U}{\partial Z}=\frac{\theta}{4(1-\mathrm{NR}_2)^2}-\frac{1}{4(1-\mathrm{NR}_2)^2}\frac{\partial P}{\partial Z}+\frac{1}{H^2}\left(\frac{\partial^2U}{\partial\eta^2}+\frac{\partial^2U}{\partial\xi^2}\right) \tag{2}$$

- Momentum equation in ξ-direction:

$$\begin{aligned}\frac{W}{H}\frac{\partial W}{\partial\xi}+\frac{V}{H^2}\frac{\partial(HW)}{\partial\eta}+4(1-\mathrm{NR}_2)^2U\frac{\partial W}{\partial Z}-\frac{V^2}{H^2}\frac{\partial H}{\partial\xi}\\=\frac{1}{H^3}\left[\frac{\partial^2(HW)}{\partial\eta^2}+\frac{\partial^2(HW)}{\partial\xi^2}\right]-\frac{2}{H^4}\left[\frac{\partial(HW)}{\partial\eta}-\frac{\partial(HV)}{\partial\xi}\right]\frac{\partial H}{\partial\eta}\\+\frac{8(1-\mathrm{NR}_2)^2}{H^2}\frac{\partial H}{\partial\xi}\frac{\partial U}{\partial Z}\end{aligned} \tag{3}$$

- Energy equation for fluid:

$$\frac{W}{H}\frac{\partial\theta}{\partial\xi}+\frac{V}{H}\frac{\partial\theta}{\partial\eta}+4(1-\mathrm{NR}_2)^2U\frac{\partial\theta}{\partial Z}=\frac{1}{Pr\,H^2}\left(\frac{\partial^2\theta}{\partial\eta^2}+\frac{\partial^2\theta}{\partial\xi^2}\right) \tag{4}$$

- Energy equation for solid walls:

$$\frac{\partial^2\theta_s}{\partial R^2}+\frac{1}{R}\frac{\partial\theta_s}{\partial R}+\frac{1}{R^2}\frac{\partial^2\theta_s}{\partial\phi^2}=0 \tag{5}$$

For outer cylinder, $\theta_s=\theta_{so}$ and R vary from $\mathrm{NR}_3=1$ to NR_4 and for inner cylinder, $\theta_s=\theta_{si}$ and R vary from NR_1 to NR_2. The continuity equation (1) subjected to the no-slip condition at the walls can be written in the following integral form:

$$\bar{U}=\frac{8(1-\mathrm{NR}_2)}{\pi(1+\mathrm{NR}_2)}\int_0^{\pi}\int_{\eta_o}^{\eta_i}UH^2\,\mathrm{d}\eta\,\mathrm{d}\xi \tag{6}$$

It is worth mentioning here that the assumption "the η-velocity component (v) is much smaller than the ξ- and z-velocity components (w and u)" led to the drop of the η-momentum (roughly the radial-like direction) equation while the ξ-momentum (roughly the azimuthal-like direction) equation remained. Certainly in the concentric annulus configuration, the radial velocity is non-zero (in the developing region) and the azimuthal velocity is identically zero. On the other hand, in the eccentric annulus case both the radial-like (the η-direction) and the azimuthal-like (the ξ-direction)

components are non-zero in the developing region. However, with very low values of eccentricity one may say, under the boundary-layer theory assumptions, that both the ξ-velocity (the azimuthal-like) component (W) and theη-velocity (the radial-like) component (V) are of lower orders of magnitude than the axial velocity component (U) and consequently, as Feldman *et al.* (1982a, b) did while handling the forced flow problem, both the η- and the ξ-momentum equations might be dropped. Nevertheless, as the eccentricity increases the value of the ξ-velocity (the azimuthal-like) component (W) increases and becomes larger than the η-velocity (the radial-like) component (V). Moreover, the dropping of the η-momentum equation does not mean that the η-velocity (the radial-like) component (V) does not exist in the developing region; it simply implies that this velocity component is of lower order of magnitude than the other two components (as can be easily seen V still exists in all the above first four governing equations of the fluid domain). Additionally, with developing confined flows in pipes, parallel-plate channels and concentric annuli, the boundary-layer theory shows that the transverse-momentum equation (radial-momentum equation, in case of pipes and annuli) is the equation that can be dropped.

Equations (1)-(5) are subject to the following boundary conditions for:

- $Z = 0$ and $\eta_o < \eta < \eta_i$, $V = W = 0$, and $U = U_o$, $P = -U_o^2$, $\theta_f = \theta_s = 0.0$;
- $Z = L$ and $\eta_o < \eta < \eta_i$, $P = 0$;
- $Z \geq 0$ and $\eta = \eta_i$ or $\eta = \eta_o$, $U = V = W = 0$;
- case (I), $\theta_{si} = 1.0$ and $\theta_{so} = 0.0$ and for case (O), $\theta_{si} = 0.0$ and $\theta_{so} = 1.0$;
- $Z > 0$ and $\xi = 0$ and π (the line of symmetry):

$$\frac{\partial V}{\partial \xi} = \frac{\partial W}{\partial \xi} = \frac{\partial U}{\partial \xi} = \frac{\partial \theta}{\partial \xi} = \frac{\partial \theta_s}{\partial \phi} = 0$$

- $Z > 0$ and $R = NR_2$ and $R = NR_3 = 1$ (i.e. the interfaces) $\theta_f = \theta_s$, continuity of temperature, and:

$$k_f\left(\frac{1}{H}\frac{\partial \theta}{\partial \eta}i + \frac{1}{H}\frac{\partial \theta}{\partial \xi}j\right) = k_s\left(\frac{\partial \theta_s}{\partial R}i + \frac{1}{R}\frac{\partial \theta_s}{\partial \phi}j\right)$$

  continuity of heat flux, where i, unit vector in the η and R directions; j, unit vector in the ξ and ϕ directions.

The use of two coordinate systems rather than one was proven to be successful in describing the conjugate problem for the forced convection case (El-Shaarawi and Haider, 2001) and consequently has been applied in the present free convection case.

In the above boundary conditions as well as the integral continuity equation (6) it has been assumed that the flow enters the channel with a flat velocity profile at a value equal to the mean axial velocity in the annular gap. For boundary-layer models of confined flows, such an irrotational, uniform velocity profile is a generally accepted assumption provided that the entrance is well rounded. Also, this assumption is best justified by the results of Dyler and Fowler (1966) who concluded that "any reasonable form of entrance velocity profile may be assumed when considering overall effects." However, the discussion presented in the next paragraph clarifies the basis upon which such assumption is dependent.

The flow is considered to originate from an infinite reservoir where the fluid has zero velocity. In this case, the fluid in this reservoir is initially irrotational; that is, its vorticity is equal to zero. Upstream of the channel entrance, it is postulated that the force field is only the gravitational field, the fluid has a constant density, and the viscous forces and the corresponding friction losses are negligible. Under such assumptions, the Bernoulli constant is the same for all the streamlines and the subsequent flow, leading to the channel inlet, will remain irrotational.

Applying Bernoulli's equation at the entrance cross section, and noting that the origin of the coordinate system is located at the inlet, shows that the dimensionless pressure defect, P, at entry is equal to $-U_o^2/2$. Assuming that the streamlines in the emerging flow are parallel, the pressure defect at the channel exit could be specified as zero. This assumption is in agreement with all previous theoretical studies and is equivalent to assuming that the flow from the outlet section is a free jet.

Also, it is important to notice that the pressure appears in the governing equations as $\partial P/\partial Z$, i.e. 1st order differentiation. Consequently, only one boundary condition for the pressure is needed not two. In this regard, it will be shown in the section pertinent to the numerical method of solution that only the initial condition for the pressure at inlet ($Z = 0$) is the one that is used. On the other hand, the boundary condition for the pressure at exit ($P = 0$ at $Z = L$) is not explicitly imposed on the solution but is only continually checked for satisfaction as the solution proceeds in the axial marching direction. The satisfaction of such a boundary condition for the pressure at exit ($P = 0$ at $Z = L$) establishes the unknown channel height (L) since the present model and method of solution are handling the confined free convection problem under consideration in an inverse manner, i.e. obtaining an unknown channel height for a given volumetric flow rate (in other words a given inlet velocity U_o). Thus, the condition for the pressure at exit ($P = 0$ at $Z = L$) is a constraint rather than being a boundary condition. For each given value of U_o (i.e. a given flow rate) in an annulus of given NR_2 and E, the numerical technique searches for the location at which such a constraint is satisfied since it establishes the unknown channel height.

Numerical analysis

The above governing equations are numerically treated using a finite-difference technique to solve for the three velocity components, pressure and temperature in the fluid field and for the temperature in the two solid cylinders. Using backward finite-differences to express all first derivatives with respect to Z and the first derivative of (HV) with respect to η in the continuity equation and replacing the second and other first order derivatives in η and ξ directions by central finite-differences, equations (1)-(6) can be written in the following finite-difference forms:

- Continuity equation:

$$\frac{H(i,j+1)\,W(i,j+1) - H(i,j-1)\,W(i,j-1)}{2\Delta\xi} + \frac{H(i,j)\,V(i,j) - H(i-1,j)\,V(i-1,j)}{\Delta\eta} + 4(1-\mathrm{NR}_2)^2 H^2(i,j)\frac{U(i,j) - U^*(i,j)}{\Delta Z} = 0 \tag{7}$$

- Z-Momentum equation:

$$\begin{aligned}
&\frac{W^*(i,j)}{H(i,j)}\frac{U(i,j+1)-U(i,j-1)}{2\Delta\xi}+\frac{V^*(i,j)}{H(i,j)}\frac{U(i+1,j)-U(i-1,j)}{2\Delta\eta}\\
&\quad+4(1-\mathrm{NR}_2)^2U^*(i,j)\frac{U(i,j)-U^*(i,j)}{\Delta Z}\\
&=-\frac{1}{4(1-\mathrm{NR}_2)^2}\frac{P(i,j)-P^*(i,j)}{\Delta Z}+\frac{\theta_{\mathrm{f}}}{4(1-\mathrm{NR}_2)^2}+\frac{1}{\left[H(i,j)\right]^2}\\
&\quad\cdot\left[\frac{U(i-1,j)-2U(i,j)+U(i+1,j)}{(\Delta\eta)^2}+\frac{U(i,j-1)-2U(i,j)+U(i,j+1)}{(\Delta\xi)^2}\right]
\end{aligned}\tag{8}$$

- ξ-Momentum equation:

$$\begin{aligned}
&\frac{W^*(i,j)}{H(i,j)}\frac{W(i,j+1)-W(i,j-1)}{2\Delta\xi}+\frac{V^*(i,j)}{(H(i,j))^2}\\
&\quad\times\frac{H(i+1,j)W(i+1,j)-H(i-1,j)W(i-1,j)}{2\Delta\eta}\\
&\quad+4(1-\mathrm{NR}_2)^2U^*(i,j)\frac{W(i,j)-W^*(i,j)}{\Delta Z}\\
&\quad-\frac{(V^*(i,j))^2}{(H(i,j))^2}\frac{H(i,j+1)-H(i,j-1)}{2\Delta\xi}\\
&=\frac{1}{(H(i,j))^3}\left\{\frac{H(i-1,j)W(i-1,j)-2H(i,j)W(i,j)+H(i+1,j)W(i+1,j)}{(\Delta\eta)^2}\right.\\
&\quad\left.+\frac{H(i,j-1)W(i,j-1)-2H(i,j)W(i,j)+H(i,j+1)W(i,j+1)}{(\Delta\xi)^2}\right\}\\
&\quad-\frac{2}{(H(i,j))^4}\left(\frac{H(i+1,j)-H(i-1,j)}{2\Delta\eta}\right)\\
&\quad\times\left\{\frac{H(i+1,j)W(i+1,j)-H(i-1,j)W(i-1,j)}{2\Delta\eta}\right.\\
&\quad\left.-\frac{H(i,j+1)V(i,j+1)-H(i,j-1)V(i,j-1)}{2\Delta\xi}\right\}\\
&\quad+\frac{8(1-\mathrm{NR}_2)^2}{(H(i,j))^2}\frac{H(i,j+1)-H(i,j-1)}{2\Delta\xi}\frac{U(i,j)-U^*(i,j)}{\Delta Z}
\end{aligned}\tag{9}$$

- Energy equation for fluid:

$$\frac{W^*(i,j)}{H(i,j)}\,\frac{\theta_{\mathrm{f}}(i,j+1)-\theta_{\mathrm{f}}(i,j-1)}{2\Delta\xi}+\frac{V^*(i,j)}{H(i,j)}\,\frac{\theta_{\mathrm{f}}(i+1,j)-\theta_{\mathrm{f}}(i-1,j)}{2\Delta\eta}$$
$$+4(1-\mathrm{NR}_2)^2U^*(i,j)\frac{\theta_{\mathrm{f}}(i,j)-\theta_f^*(i,j)}{\Delta Z}$$
$$=\frac{1}{Pr(H(i,j))^2}\left(\frac{\theta_{\mathrm{f}}(i-1,j)-2\theta_{\mathrm{f}}(i,j)+\theta_{\mathrm{f}}(i+1,j)}{(\Delta\eta)^2}\right.$$
$$\left.+\frac{\theta_{\mathrm{f}}(i,j-1)-2\theta_{\mathrm{f}}(i,j)+\theta_{\mathrm{f}}(i,j+1)}{(\Delta\xi)^2}\right) \tag{10}$$

- Energy equation for outer solid wall:

$$\frac{\theta_{\mathrm{so}}(i+1,j)-2\theta_{\mathrm{so}}(i,j)+\theta_{\mathrm{so}}(i-1,j)}{(\Delta R_{\mathrm{o}})^2}$$
$$+\frac{1}{[\mathrm{NR}_4-(i-1)\Delta R_{\mathrm{o}}]}\,\frac{\theta_{\mathrm{so}}(i+1,j)-\theta_{\mathrm{so}}(i-1,j)}{2\Delta R_{\mathrm{o}}} \tag{11}$$
$$+\frac{1}{\left[\mathrm{NR}_4-(i-1)\Delta R_{\mathrm{o}}\right]^2}\,\frac{\theta_{\mathrm{so}}(i,j+1)-2\theta_{\mathrm{so}}(i,j)+\theta_{\mathrm{so}}(i,j-1)}{(\Delta\phi)^2}=0$$

- Energy equation for inner solid wall:

$$\frac{\theta_{\mathrm{si}}(i+1,j)-2\theta_{\mathrm{si}}(i,j)+\theta_{\mathrm{si}}(i-1,j)}{(\Delta R_{\mathrm{i}})^2}$$
$$+\frac{1}{\left[\mathrm{NR}_2-(i-1)\Delta R_{\mathrm{i}}\right]}\,\frac{\theta_{\mathrm{si}}(i+1,j)-\theta_{\mathrm{si}}(i-1,j)}{2\Delta R_{\mathrm{i}}} \tag{12}$$
$$+\frac{1}{\left[\mathrm{NR}_2-(i-1)\Delta R_{\mathrm{i}}\right]^2}\,\frac{\theta_{\mathrm{si}}(i,j+1)-2\theta_{\mathrm{si}}(i,j)+\theta_{\mathrm{si}}(i,j-1)}{(\Delta\phi)^2}=0$$

- Integral form of the continuity equation:

$$\bar{U}=\frac{8(1-\mathrm{NR}_2)}{\pi(1+\mathrm{NR}_2)}\left(\sum_{j=2}^{M}\sum_{i=2}^{N}U(i,j)\big(H(i,j)\big)^2+0.5\sum_{i=2}^{N}U(i,1)\big(H(i,1)\big)^2\right.$$
$$\left.+U\big(i,M+1\big)\big(H\big(i,M+1\big)\big)^2\right)\Delta\eta\Delta\xi \tag{13}$$

The finite-difference equations (8)-(10) are linearized by assuming that, where ever the product of two unknowns occur, one of them is given approximately by its value at the previous axial step, the variable subscripted with an asterisk (*). Moreover, in equation (9), the finite difference representation of the ξ-momentum equation (3), all

the values of V have been deliberately taken at the previous axial step. This makes equation (9) locally (i.e. within one axial step) uncoupled from the continuity equation (7) and makes the finite-difference equations (7)-(13) represent a complete mathematical model of seven equations in seven unknowns (U, V, W, P, θ_f, θ_{si}, θ_{so}). Hence, it enables these equations to be numerically solved in the manner described later in the next section. The dependent variables (U, V, W, P, θ_f, θ_{si}, θ_{so}) are computed, for each vertical (axial) location (Z) at the intersections of the grid lines, i.e. the mesh points. The solution progresses from the lower entrance of the channel to its upper exit in axial steps, the size of which increases with Z.

One may raise the issue that the integral form of the continuity equation (6) is not an independent equation. In fact, equation (6) is simply an integrated form of equation (1) subject to the appropriate boundary conditions. Thus, equations (1) and (6) are not independent and in the fluid domain there are five variables (U, V, W, P and θ). Owing to the dropping of the η-momentum equation, there are only four governing equations (1 to 4; the continuity, axial-momentum, ξ-momentum, and energy equations) and their finite-difference forms (7)-(10). Therefore, it may appear that we are solving four equations in five unknowns and contradicting a rule of thump that the number of equations should equal the number of unknowns. This issue can be clarified by one of the two following arguments.

Firstly, one should notice that the linearized numerical technique used here depends, as stated above, on the use of the values of U, V and W in the coefficients of the convective terms (on the left hand sides of equations (2)-(4)) as taken from the preceding axial step. In other words, within each axial step, the values of U, V and W in the coefficients of the convective terms (on the left hand sides of equations (2)-(4)) are assumed constants at their previous values (at the preceding axial station). Accordingly, this linearization technique enables the decoupling, within each axial step, of the energy equations (4) and (5) from the momentum and continuity equations. This in turn enables the numerical solution of the energy equations in the fluid and solid domains first within each axial step. Thus, the numerical solution starts by solving the energy equations (4) and (5) to obtain the values of θ_f and θ_s at the second axial station. With these obtained values of θ_f and the known linearized coefficients U, V and W on the left hand side of equation (3), the integral continuity equation (6) together with the linearized axial momentum equation (3) become two equations in the two unknowns U and P. Thus, equations (3) and (6) can be numerically solved to obtain the values of U and P at the second axial station. Now, with the obtained values of U and the known linearized coefficients U, V and W on the left hand side of equation (2) as well as all other values of V on the right hand side of equation (2) to be taken from the preceding axial step, the ξ-momentum equation (2) can be solved on its own to get the values of W at the second axial station. Then, the application of a numerical form of the differential continuity equation (1) at the second cross section using the already obtained values of U and W will allow the solution for the values of V at this second cross-section. Repeating this process at each next axial step allows a marching solution for the governing parabolic differential equations.

Secondly, the four equations in the fluid domain, with the assumption that pressure is only a function of Z, plus an "extra" boundary condition for V, are sufficient to solve for the five unknowns. The system of equations we use has only a first order derivative of V with respect to η; therefore it can only support a single η-direction boundary

condition of V. By imposing two such boundary conditions (zero velocity at both walls) one has an additional piece of information that makes the system of equations complete.

Thermal boundary conditions are imposed on the inner surface of the inner cylinder and the outer surface of the outer cylinder. The thermal conditions at the two fluid-wall interfaces are not known; they depend on the properties and flow characteristics of the fluid as well as the dimensions and properties of the solid walls. Having the governing equations for the fluid in bipolar coordinates and the energy equations for the solid walls in cylindrical coordinates generates unmatched grid points on both the interfaces. Continuity of temperature and heat flux at the solid fluid interfaces provides the necessary link. Equations representing the continuity of temperature and heat flux are applied to determine the thermal conditions on the cylindrical mesh points at each of the solid-fluid interfaces whereas interpolation equations are applied to calculate the temperature on the bipolar mesh points at each of the interfaces. At the interface points, continuity of temperature and continuity of heat flux can be expressed in finite-difference forms as follows.

At the corner points I through IV, shown in Figure 2, continuity of temperature and heat flux are expressed by the following relations, in which b, n, c and s are numerical indices replacing the index i at these corners; the first pair (b and n) in the fluid zone and the second pair (c and s) in the solid zone, respectively.

At $\xi = 0$ (Widest Gap, $j = 1$) [Points I (on outer interface) and II (on inner interface)]

$$\begin{aligned} \theta_f(b+1,1) &= \theta_s(s+1,1), \\ \mathrm{KR}^* H(b+1,1)\left[\frac{\theta_s(c+1,1)-\theta_s(c,1)}{\Delta R}\right] &= \frac{\theta_f(n+1,1)-\theta_f(n,1)}{\Delta\eta} \end{aligned} \tag{14}$$

At $\xi = \pi$ (Narrowest Gap, $j = M + 1$) [Points III (on inner interface) and IV (on outer interface)]

$$\begin{aligned} &\theta_f(b+1,M+1) = \theta_s(s+1,M+1), \\ &\mathrm{KR}^* H(b+1,M+1)\left[\frac{\theta_s(c+1,M+1)-\theta_s(c,M+1)}{\Delta R}\right] \\ &\quad = \frac{\theta_f(n+1,M+1)-\theta_f(n,M+1)}{\Delta\eta} \end{aligned} \tag{15}$$

The continuity of temperature and heat flux on rest of the mesh points ($2 \le j \le M$) are expressed using the following relations:

$$\theta_f(b+1,j) = \theta_s(s+1,j),$$

$$\theta_f(b+1,j+1) = \theta_s(s+1,j+1),$$

$$\theta_f(b+1,j-1) = \theta_s(s+1,j-1),$$

$$\mathrm{KR}^{*}H(b+1,j)\left[\frac{\theta_{\mathrm{s}}(c+1,j)-\theta_{\mathrm{s}}(c,j)}{\Delta R}+\frac{1}{\mathrm{NR}}\,\frac{\theta_{\mathrm{s}}(s+1,j+1)-\theta_{\mathrm{s}}(s+1,j-1)}{2\Delta\phi}\right] = \frac{\theta_{\mathrm{f}}(n+1,j)-\theta_{\mathrm{f}}(n,j)}{\Delta\eta}+\frac{\theta_{\mathrm{f}}(b+1,j+1)-\theta_{\mathrm{f}}(b+1,j-1)}{2\Delta\xi} \tag{16}$$

where $2 \le j \le M$

In equations (14)-(16):

$$\theta_{\mathrm{s}} = \theta_{\mathrm{so}} \quad \text{(For outer interface)} \qquad \theta_{\mathrm{s}} = \theta_{\mathrm{si}} \quad \text{(For inner interface)}$$

$$\Delta R = \Delta R_{\mathrm{o}} \quad \text{(For outer interface)} \qquad \Delta R = \Delta R_{\mathrm{i}} \quad \text{(For inner interface)}$$

$$\mathrm{NR} = \mathrm{NR}_3 \quad \text{(For outer interface)} \qquad \mathrm{NR} = \mathrm{NR}_2 \quad \text{(For inner interface)}$$

The values of the numerical indices b, c, n, and s are:

$$b = o \quad \text{(For outer interface)} \qquad b = N \quad \text{(For inner interface)}$$

$$C = \mathrm{NSO} \quad \text{(For outer interface)} \qquad c = 1 \quad \text{(For inner interface)}$$

$$n = 1 \quad \text{(For outer interface)} \qquad n = N \quad \text{(For inner interface)}$$

$$s = \mathrm{NSO} \quad \text{(For outer interface)} \qquad s = 0 \quad \text{(For inner interface)}$$

Interpolation of temperature on interfaces

At both interfaces, temperature at every mesh point of the bipolar grid is evaluated by interpolation relations using the temperatures at the two neighboring mesh points of the cylindrical grid. The x-coordinate of the grid points is used for this purpose. This interpolation can be expressed as follows (Figure 2).

Fluid temperatures on the outer interface

$$\theta_{\mathrm{f}}(1,j) = \theta_{\mathrm{so}}(\mathrm{NSO}+1,jj) + \left[\theta_{\mathrm{so}}(\mathrm{NSO}+1,jj+1) - \theta_{\mathrm{so}}(\mathrm{NSO}+1,jj)\right] \times \left[\frac{X_{\mathrm{f}}(1,j)-X_{\mathrm{so}}(1,jj)}{X_{\mathrm{so}}(1,jj+1)-X_{\mathrm{so}}(1,jj)}\right] \tag{17}$$

Fluid temperatures on the inner interface

$$\theta_{\mathrm{f}}(N+1,j) = \theta_{\mathrm{si}}(1,jj) + \left[\theta_{\mathrm{si}}(1,jj+) - \theta_{\mathrm{si}}(1,jj)\right]\left[\frac{X_{\mathrm{f}}(N+1,j)-X_{\mathrm{si}}(1,jj)}{X_{\mathrm{si}}(1,jj+1)-X_{\mathrm{si}}(1,jj)}\right] \tag{18}$$

Method of solution

In practice, the dimensions of the channel (l and D) and ambient temperature are normally known while the volumetric flow rate f is unknown. However, the present model and method of solution are handling the problem in a reverse manner,

i.e. obtaining an unknown dimensionless channel height (L) for a given dimensionless volumetric flow rate (F). Therefore, the condition $P = 0$ at $Z = L$ is not explicitly imposed on the solution, but continually checked for satisfaction; recall that the governing equations (1)-(6) are parabolic in Z and need only one condition with respect to Z. Owing to symmetry, these equations need to be solved in only half of the domain, i.e. for $0 \leq \xi \leq \pi$. The problem under investigation is governed by seven dimensionless parameters, namely, the fluid annulus radius ratio (NR_2), the eccentricity (E), the Prandtl number (Pr), inlet fluid velocity (U_o), conductivity ratio (KR) and thicknesses of the two walls (δ_o and δ_i).

For a fluid of a given Pr in an annulus of given NR_2 and E, the solution starts by calculating the corresponding values of η_i and η_o by means of the relations given in the nomenclature. Selecting the numbers of increments in η and ξ directions (N and M, respectively) the values of $\Delta\eta$ and $\Delta\xi$ can be computed by using the relations given in the nomenclature. Similarly, for the solid walls, by selecting the values of NR_1 and NR_4 and the number of radial increments in the outer and inner walls and the number of increments in the tangential (ϕ) direction (NSO, NSI and M, respectively), the values of ΔR_o, ΔR_i and $\Delta\phi$ can be determined. Assume a value for the uniform axial velocity at the entrance U_o (i.e. F since $F = U_o(1 - NR_o^2)$, the inlet pressure will be $P_o = -U_o/2$, since $W = V = 0$.

For each axial location (cross-section), the energy equations for the fluid (equation (10)) and solids (equations (11) and (12)) are simultaneously solved for the temperatures using Gauss-Seidel iteration. The solution starts by simultaneously solving equations (10)-(12) to obtain the unknown values of θ_f, θ_{si} and θ_{so}. Within the Gauss-Seidel iteration process, the temperature values of the cylindrical grid points at the two interfaces are calculated using the principles of continuity of temperature and heat flux. The temperature values of the bipolar grid points at both the interfaces are computed by interpolating between the temperature values of the two neighboring cylindrical grid points at both sides of each bipolar grid point. To solve for the two unknowns P and U at the aforesaid axial location, the integral form of the continuity equation (13) and the finite-difference form of the axial-momentum equation (8) are used. The resulting set of algebraic equations is solved by a modified Gauss-Jordan elimination scheme. Then ξ-Momentum equation (9) is solved for W-velocity component using Gauss-Seidel iteration method. Finally, the continuity equation (7) is used to evaluate V-component of velocity at all the interior grid points. These steps are repeated to advance axially until the pressure defect (P) becomes zero indicating that the channel exit has been reached and consequently the value of L is determined.

Results and discussion

Owing to the neglect of the axial diffusion terms ($\partial^2/\partial Z^2 = 0$), and the neglect of the variations of pressure with the two transverse directions ($\partial P/\partial\eta = \partial P/\partial\xi = 0$), the Grashof number is inherent in the dimensionless formulation of the problem ($Gr* = GrD_h/l$) and thus it is not explicitly needed for the solution. However, seven other similarity parameters are explicitly required to solve the problem under consideration. These are the fluid annulus radius ratio (NR_2), the dimensionless eccentricity (E), the dimensionless flow rate F (or effectively $U_o = F/(1 - NR_2^2)$), solid-fluid thermal conductivity ratio (KR), inner and outer cylinder walls thickness (δ_i and δ_o) and the Parandtl number (Pr). However, one should recall that the inlet

velocity (U_o) and hence the inlet pressure (P_o) and the volumetric flow rate (F) are not predetermined initial conditions independent of the channel height as in the case of forced flows. Rather, each of them is dependent on the channel height (L) and the applied thermal boundary conditions on the annulus walls. The numerical results to be presented in this paper are for a fluid of $Pr = 0.7$ in an annulus of cylinders having walls thicknesses $\delta_i = 0.1$ and $\delta_o = 0.2$.

First of all, numerical experiments have been conducted to reach a mesh-independent solution. In this regard, 12 different mesh sizes for the fluid annulus and inner and outer solid walls were tested. Among all, the mesh sizes of 25×25 (in η and ξ directions), 20×25 (in r and (ϕ directions) and 10×25 (in r and (ϕ directions) for the fluid annulus, outer cylinder wall and inner cylinder wall, respectively, were selected; representing the best compromise between time of execution of the program and percentage difference (less than 1 percent in the value of each of the inner wall heat at exit ($HF_{i,ex}$), the outer wall heat flux at exit ($HF_{o,ex}$), the exit Nusselt number on the inner wall ($Nu_{i,ex}$), etc). Table I shows a summary for some of these numerical experiments, taking the 30×30 mesh as the reference. On the other hand, it is known that near the annulus entrance large gradients exist. For, this reason all the computer runs were made by taking very small steps near the entrance. Further, downstream the axial step was increased several times as the flow moves away from the entrance.

To check the adequacy of the present results, special runs were carried out simulating the three different limiting cases of: conventional forced convection, conjugate forced convection and conventional natural convection in the given eccentric annuli. For both the conventional forced and the conventional natural convection cases, the present computer code was made to run at very large values of solid-fluid thermal conductivity ratio (KR = 1,000) and very thin cylinder walls ($\delta_i = 0.001$ and $\delta_o = 0.002$); thus the conjugate effect could be negligible. On the other hand, the present computer code can simulate the forced convection cases (conventional or conjugate) when the values of the inlet velocity U_o exceeds the corresponding limiting values for natural convection (El-Shaarawi *et al.*, 2001). The results and conclusions of these special computer-code runs are as follows.

First, comparisons between the fully-developed forced convection pressure gradient and heat transfer results available in the literature and the corresponding conventional results (without conjugation) obtained by special runs of the present computer code revealed that the maximum deviations between the obtained results and those reported by Trombetta (1972), El-Shaarawi and Haider (2001) and Shah and London (1978) were 0.36, 0.12 and 1.34 percent, respectively, as shown in Table II. Moreover, the present special computer-code results were also checked with the conventional forced convection results obtained by El-Shaarawi *et al.* (1998) for the fully developed mixed-mean temperature ($\theta_{m,fd}$); the maximum percentage difference was found to be 0.032 percent.

Secondly, the present computer code was validated for the conjugate forced convection case in eccentric annuli by comparing the results obtained from a pertaining special run with the corresponding developing and fully developed temperature profiles across the widest gap ($\Psi = 0$) of El-Shaarawi and Haider (2001); excellent agreement was observed as the maximum deviation between the obtained results and those of El-Shaarawi and Haider (2001) never exceeded 0.23 percent.

Parameters		Fluid-annulus mesh ($N \times M$)					Solid-walls mesh (NSI and NSO)				
		20 × 25	25 × 25	25 × 30	30 × 25	30 × 30	20 and 25	25 and 25	25 and 30	30 and 25	30 and 30
$HF_{i,ex}$	Value	2.944	2.946	2.946	2.949	2.949	2.948	2.947	2.949	2.946	2.948
	Percentage of diff.	0.172	0.097	0.095	0.000		0.001	0.021	0.040	0.060	
$HF_{o,ex}$	Value	−1.468	−1.467	−1.467	−1.466	−1.466	−1.467	−1.467	−1.468	−1.466	−1.467
	Percentage of diff.	0.178	0.101	0.098	0.001		0.046	0.012	0.055	0.042	
$Nu_{i,ex}$	Value	5.055	5.051	5.051	5.049	5.049	5.049	5.046	5.045	5.041	5.041
	Percentage of diff.	0.115	0.036	0.035	0.002		0.155	0.098	0.093	0.005	
$Nu_{o,ex}$	Value	3.516	3.521	3.521	3.524	3.524	3.527	3.527	3.532	3.528	3.533
	Percentage of diff.	0.225	0.087	0.085	0.002		0.171	0.156	0.020	0.134	
$\theta_{m,ex}$	Value	0.418	0.417	0.417	0.416	0.416	0.416	0.416	0.415	0.416	0.415
	Percentage of diff.	0.403	0.187	0.183	0.003		0.217	0.169	0.075	0.092	
Z_{ex}	Value	0.006	0.007	0.007	0.007	0.007	0.007	0.007	0.007	0.007	0.007
	Percentage of diff.	18.677	9.338	9.338	0.000		1.408	1.408	0.000	0.000	
No. of steps	Value	179.000	186.00	186.00	193.00	193.00	188.00	188.00	189.00	189.00	189.00
	Percentage of diff.	7.254	3.627	3.627	0.000		0.529	0.529	0.000	0.000	
Time (min.)	Value	7.643	13.015	21.751	22.525	35.346	15.149	16.575	17.113	18.237	18.675
	Percentage of ratio	21.623	36.821	61.537	63.728		81.122	88.755	91.638	97.657	

Table I.
Summary of the numerical experiments for grid independent solution

Parameters/models	Present	El-Shaarawi and Haider (2001)	Percentage of error	Present		Percentage of error
				Shah and London (1978)		
$(dp/dz)_{fd}$	32.2466	32.2070	0.1229	32.2466	31.8180	1.3470
					Trombetta (1972)	
$HF_{i,fd}$	3.5948	3.5930	0.0500	3.5948	3.5820	0.3573
$\overline{Nu}_{i,fd}$	5.7407	5.7380	0.0468	5.7407	5.7460	0.0925
$\overline{Nu}_{o,fd}$	4.7616	4.7620	0.0077	4.7616	4.7540	0.1606
Configuration						
$NR_1 = 0.499$, $N = 20$						
$NR_2 = 0.5$, $M = 20$						
$NR_4 = 1.002$, NSI = 8						
KR = 1,000, NSO = 16						
$E = 0.6$, Case = 1.I						
$Pr = 0.7$, Forced convection						

Table II.
Comparison with available results for eccentric annuli

In the context of the above comparisons with forced convection results, one should mention that in the forced-convection simulations there is no check on the value of the dimensionless pressure with axial location (as in the free convection case); indeed the dimensionless pressure continues is such forced flow cases to decrease in value without any possibility of recovering back as occurs in the free convection flow.

Thirdly, a special computer run simulating the conventional natural convection case was done. The obtained results for the channel height required to suck specific flow rates under thermal boundary conditions of the first kind are compared in Figure 4 with the corresponding results of El-Shaarawi and Mokheimer (1999).

In order to show the conjugation effect on the heat transfer results, computer runs were conducted for very thin walls, representing the conventional case, and very thick walls, representing the conjugate case, at different values of eccentricity (E) and radius ratio (NR_2). Figure 5 shows the induced flow rate (F) plotted against the eccentricity for very thin walls ($\delta_i = 0.001$, $\delta_o = 0.002$) and very thick walls ($\delta_i = 0.2$, $\delta_o = 0.4$) for $L = 5 \times 10^{-3}$. Another comparison is made in Figure 6 to show the effect of radius ratios NR_2. It is evident from these two figures that the conjugation effect cannot be ignored in such cases. However, it is worth mentioning that the curves for thick and thin walls in Figure 6 are closer to each other as compared to the curves in Figure 5. This is because Figure 6 considers the thick walls as $\delta_i = 0.15$ and $\delta_o = 0.3$, which is less than the thickness that has been taken in Figure 5, i.e. $\delta_i = 0.2$ and $\delta_o = 0.4$, due to limitations on the annulus geometry at very large and very small values of radius ratio (NR_2). From these results, one can anticipate similar behavior for very large and small values of thermal conductivity ratio (KR), representing the conventional and conjugate cases, respectively.

A comparison between the conjugate and conventional results for the parameters L, $\bar{Q}$, $\overline{Nu}_{i,e}$ and $\overline{Nu}_{o,e}$ is presented in Table III. The table shows that the percentage

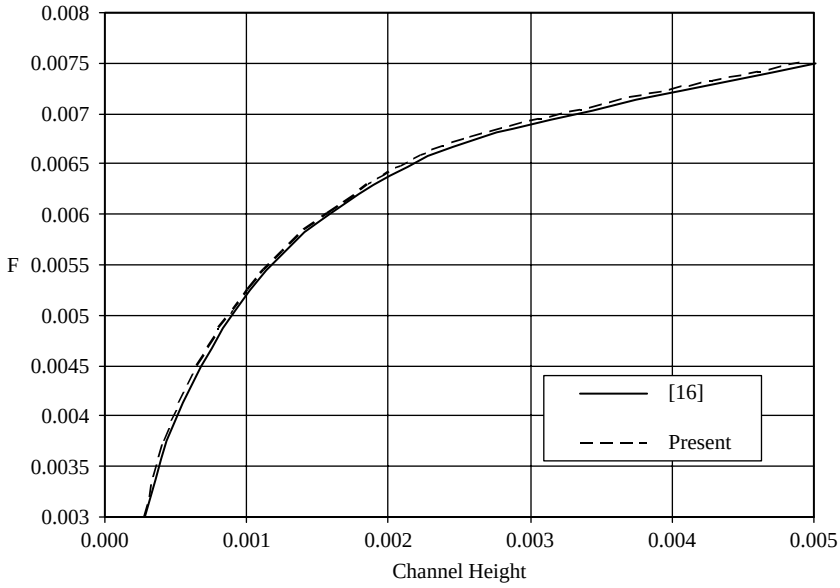

Figure 4.
Comparison of volumetric flow rate versus channel height as reported by El-Shaarawi and Mokheimer (1999) and the corresponding results by a special computer run simulating conventional free convection, $N = 20$, $M = 20$, $Pr = 0.7$, $NR_1 = 0.499$, $NR_2 = 0.5$, $NR_3 = 1.0$, $NR_4 = 1.002$, KR = 1,000, NSI = 25, NSO = 25

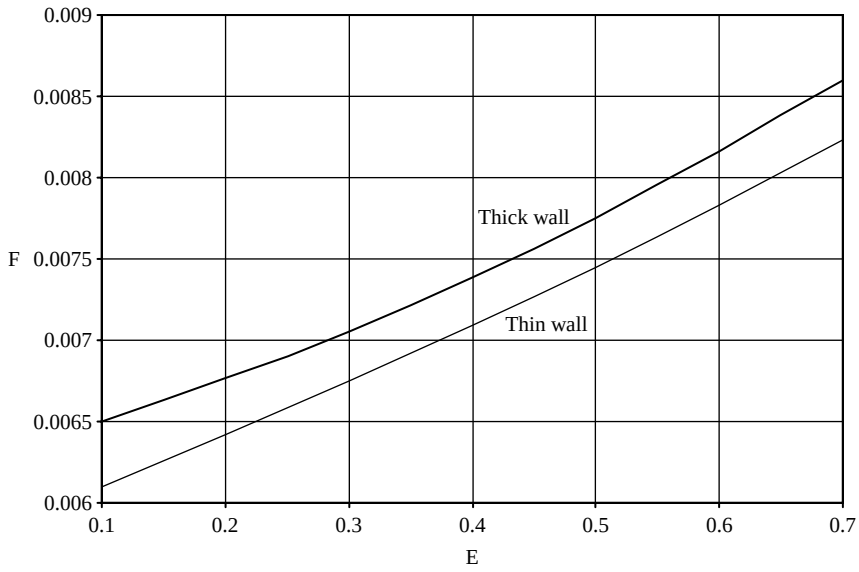

Figure 5.
Variation of flow rate with eccentricity for thick walls ($\delta_i = 0.2$, $\delta_o = 0.4$) and thin walls ($\delta_i = 0.001$, $\delta_o = 0.002$) $NR_2 = 0.5$, $Pr = 0.7$, Height $(L) = 5 \times 10^{-3}$, KR = 1, Case (I)

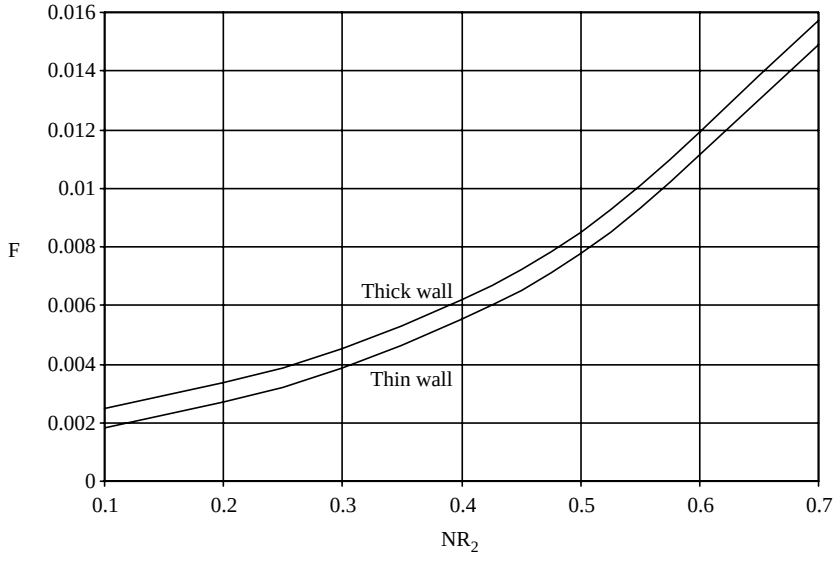

Figure 6.
Variation of flow rate with radius ratio for thick walls ($\delta_i = 0.15$, $\delta_o = 0.3$) and thin walls ($\delta_i = 0.001$, $\delta_o = 0.002$) $E = 0.5$, $Pr = 0.7$, Height $(L) = 8 \times 10^{-3}$, KR = 1, Case (I)

difference between the conjugate and conventional free convection results ranges from 0.1619 to 26.602 percent. Such percentage differences are also shown graphically in Figure 7. This figure clearly indicates that increasing E increases the percentage differences and this clearly supports the fact that conjugation effects increase with E.

Figures 8 and 9 show the important variation of induced flow rate with the channel height for different values of the eccentricity for cases (I) and (O), respectively. It can be

E	$U_o \times 10^3$	$F \times 10^4$	$L \times 10^5$ Conj.	$L \times 10^5$ Conv.	$\bar{Q} \times 10^4$ Conj.	$\bar{Q} \times 10^4$ Conv.	$\overline{Nu}_{i,e}$ Conj.	$\overline{Nu}_{i,e}$ Conv.	$\overline{Nu}_{o,e}$ Conj.	$\overline{Nu}_{o,e}$ Conv.
$E = 0.1$	3.5	26.25	19.2	17.5	10.52	10.80	5.64756	6.44226	2.35572	2.52587
	4.0	30	25.1	24.0	12.20	12.60	5.34803	6.12708	2.46837	2.64127
	5.0	37.5	42.1	36.0	15.82	15.20	5.06524	5.95278	2.65058	2.72283
	6.0	45	70.7	65.0	19.40	19.00	4.89792	5.62494	2.76790	2.98279
	7.0	52.5	125.2	116.0	22.73	22.50	4.79550	5.40027	2.83662	3.13310
	8.0	60	265.7	260	25.78	25.50	4.74238	5.39579	2.87443	3.20440
$E = 0.5$	4.0	30	32.1	28.5	12.12	12.00	5.49076	6.982	2.94044	3.575
	5.0	37.5	48.8	43.6	14.90	14.60	5.26770	6.240	3.05893	3.563
	6.0	45	74.2	67.5	18.20	17.90	5.17945	6.107	3.13193	3.622
	7.0	52.5	113.1	102.0	21.53	21.40	5.11771	6.045	3.18674	3.669
	8.0	60	175.5	158.0	24.74	24.70	5.06404	5.955	3.22938	3.739
$E = 0.7$	3.5	26.25	23.5	24.1	10.86	11.40	7.53536	9.0083	3.76209	4.0521
	4.0	30	35.7	32.1	12.10	12.80	5.93964	8.0924	3.38149	4.2705
	5.0	37.5	53.1	46.0	14.40	14.10	5.63350	7.2976	3.54016	4.5904
	6.0	45	76.6	68.0	17.32	16.90	5.54798	7.0683	3.59773	4.6493
	7.0	52.5	109.2	98.0	20.50	20.10	5.51193	7.0450	3.62361	4.6391
	8.0	60	155.3	141.0	23.74	23.50	5.48860	7.0479	3.64324	4.6302

Notes: Fixed parameters: $NR_2 = 0.5$, $KR = 10$, $\delta_i = 0.1$, $\delta_o = 0.2$, Case (I)
Source: Mokheimer (1996)

Table III.
Values of L,$\bar{Q}$, $\overline{Nu}_{i,e}$, and $\overline{Nu}_{o,e}$ for conjugate and conventional cases at different values of E

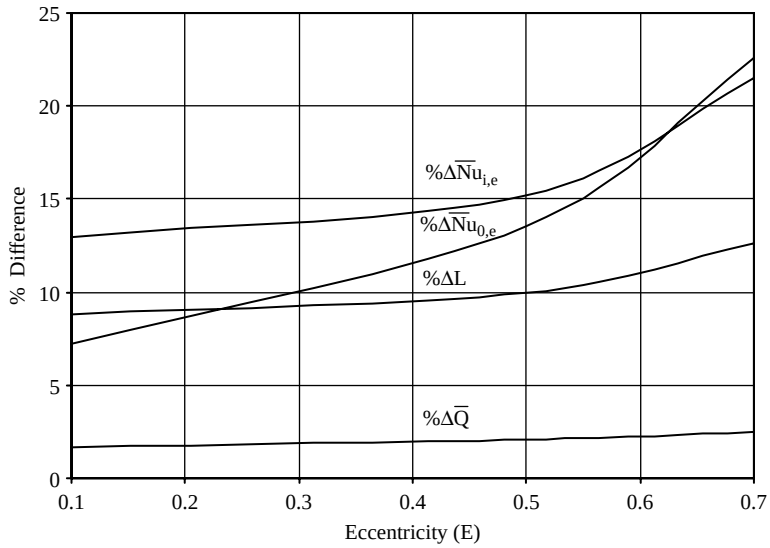

Figure 7.
Percentage difference between conjugate and conventional cases for different parameters ($\bar{Q}$, L, $\overline{Nu}_{i,e}$, $\overline{Nu}_{o,e}$) (Case I) $NR_2 = 0.5$, $KR = 10$, $\delta_i = 0.1$, $\delta_o = 0.2$, $F = 0.0045$

seen from the comparison shown in Figure 10 that, for a given channel height, the flow rate induced is greater for case (O) than that for case (I). This can be attributed to the larger heating surface in case (O) than that in case (I). In both cases (I and O), for given radius ratio, conductivity ratio and channel height, increasing the eccentricity increases the induced flow rate. A large value of eccentricity increases the velocity

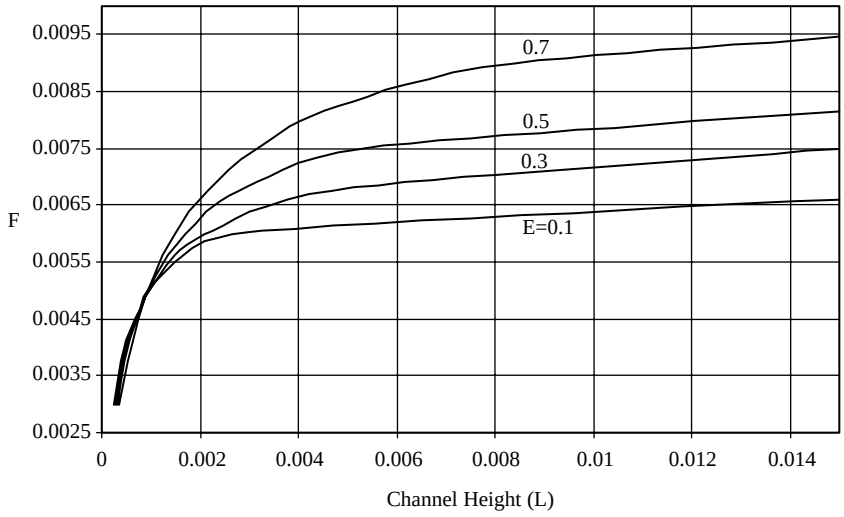

Figure 8.
Variation of flow rate with channel height for different values of eccentricity (Case I)

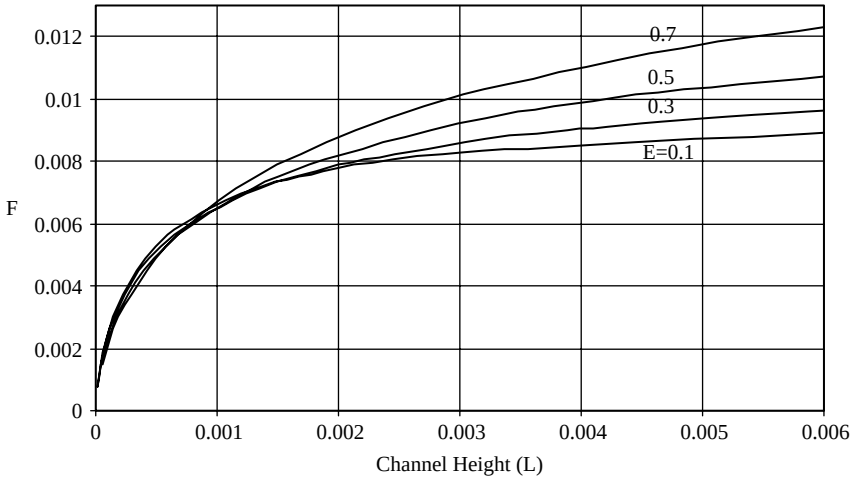

Figure 9.
Variation of flow rate with channel height for different values of eccentricities (Case O) $NR_2 = 0.5$, $\delta_i = 0.1$, $\delta_o = 0.2$, KR = 10

asymmetry, which causes the resistance of flow to increase/decrease on the narrowest ($\psi = 1$)/widest ($\psi = 0$) gap side of the annulus. The axial velocity profile develops with increasing/decreasing values on the widest ($\psi = 0$)/narrowest ($\psi = 1$) gap side of the annulus resulting in a net increase in average velocity and a higher heat transfer coefficient. This is mainly due to the increase in heat transfer to the fluid by convection in the widest gap ($\psi = 0$). Consequently, the mean fluid temperature increases leading to an increased flow rate. However, for very short channels in both cases (I and O) a reverse trend occurs, i.e. increasing the eccentricity decreases the induced flow rate. The reason is that for short channels with a large eccentricity, the axial velocity and temperature profiles do not develop sufficiently. This consequently reduces the mean bulk temperature (i.e. reduction of the buoyancy forces) and the induced flow rate.

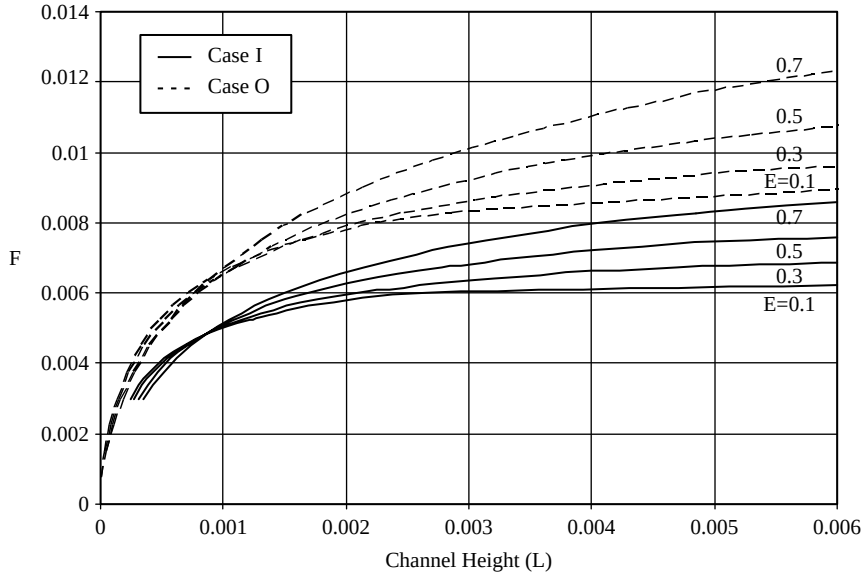

Figure 10.
Comparison of flow rate with channel height for different eccentricities for cases (I) and (O) $NR_2 = 0.5$, $\delta_i = 0.1$, $\delta_o = 0.2$, KR $= 10$

In the current problem the heat transfer from the hot surface is divided between the cold surface and flowing fluid. Consequently, in the present situation there is no single Nusselt number that can be correlated versus Rayleigh number as in the simple cases of tube and flat plate. Accordingly, in the present work two Nusselt numbers are used for the heat transfer through the inner and outer surfaces that bound the fluid annulus (Nu_i and Nu_o, respectively) in addition to the total heat absorbed by the fluid ($\bar{Q}$) as it passes through the annulus. The latter is frequently more important to engineers and is therefore usually reported in the free convection literature. Figure 11 shows the total heat absorbed by the fluid ($\bar{Q}$) for case (I) versus the channel height (L) for four

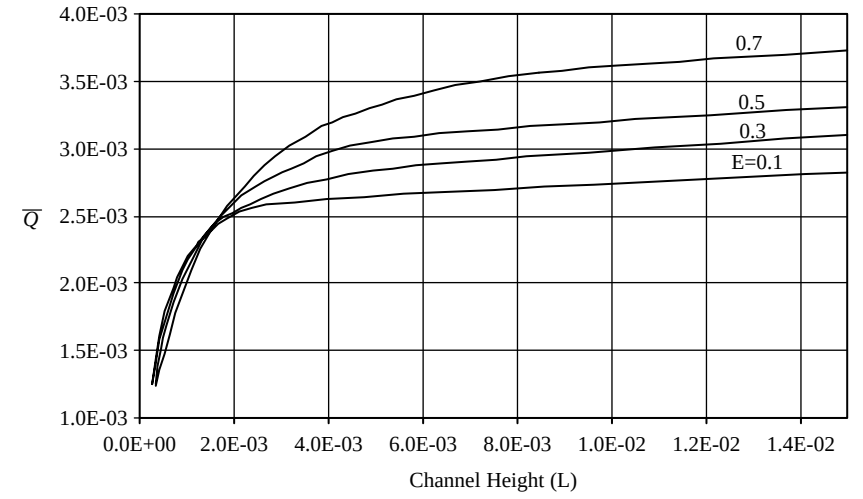

Figure 11.
Total heat absorption versus channel height for different values of eccentricity (Case I) $NR_2 = 0.5$, $\delta_i = 0.1$, $\delta_o = 0.2$, KR $= 10$

dimensionless eccentricities. Taking into consideration that L is the reciprocal of the modified Grashof number (Gr^*) and that Pr is constant (0.7) in the present work, so the abscissa of Figure 11 is related to the modified Rayeigh number ($Gr^* \times Pr$). As can be seen from this figure, the higher the value of the eccentricity for short channels the less amount of heat gained by the fluid. This trend reverses for high channels (large values of L). These are also true for case (O) as can be seen from Figure 12. Again, the reason is that for high channels (large values of L), when the eccentricity increases, the fluid flow at the widest gap side of the annulus develops with higher values of velocity as compared to the narrowest gap (because the widest gap offers less resistance to fluid flow). This increases the coefficient of heat transfer on the widest gap side and enhances the ability of fluid to absorb more heat, thus causing more flow rate to be induced in the channel. The opposite happens for short channels since the flow does not find enough channel height to develop sufficient buoyancy effect to gain more velocity in the widest gap ($\psi = 0$) as eccentricity increases; this results in a decrease in the heat absorbed by the fluid and directly affects the induced flow rate.

Figures 13 and 14 show the effect of the annulus radius ratio (NR_2) on the dimensionless flow rate for case (I). For given eccentricity, wall thicknesses and conductivity ratio, increasing the annulus radius ratio increases the dimensionless flow rate. Similar trends have also been obtained for case (O), as can be seen in Figure 15. Such an increase in the dimensionless flow rate can be helpful in the cooling of channels having the same conductivity ratio and walls thickness.

A fluid annulus radius ratio (NR_2) is the ratio of the outer radius of the inner cylinder to the inner radius of the outer cylinder (r_{oi}/r_{io}). Therefore, an increase in this radius ratio might imply a decrease in the annulus cross sectional area and consequently smaller dimensional flow rate. This is clarified for cases (I) and (O) in Figure 16 by converting the dimensionless flow rate into its dimensional form ($f = \pi\gamma Gr(r_{io} - r_{oi})F$), for a value of Gr in the laminar range, $Gr = 10^6$, and plotting it against the radius ratio. On the other hand, increasing the radii r_{oi} and r_{io} in such a manner that the radius ratio remains constant, increases the annulus cross sectional area and hence the dimensional flow rate, which cannot be explained by Figure 16.

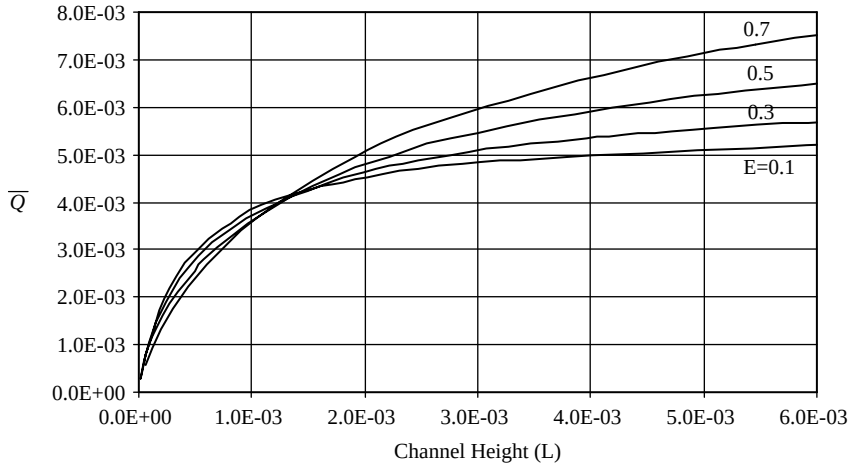

Figure 12.
Total heat absorption versus channel height for different values of eccentricity (Case O) $NR_2 = 0.5$, $\delta_i = 0.1$, $\delta_o = 0.2$, KR $= 10$

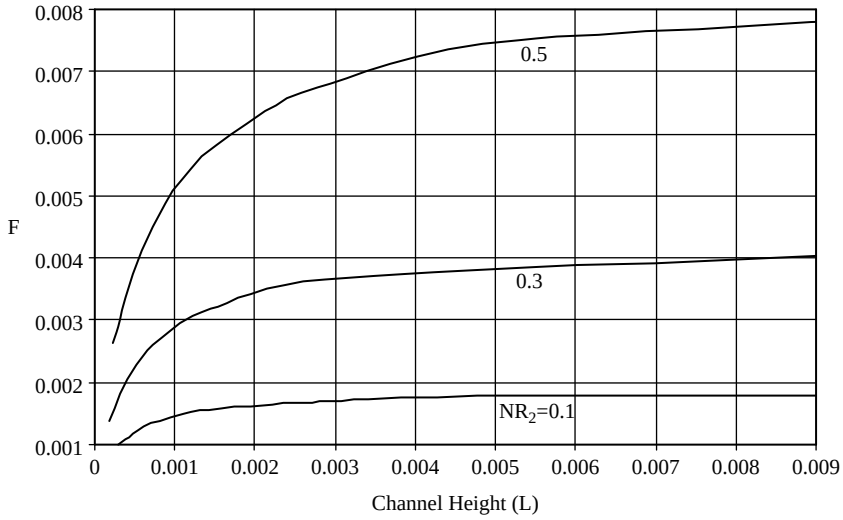

Figure 13.
Variation of flow rate with channel height for different values of radius ratio (Case I) KR = 10, $\delta_i = 0.1$, $\delta_o = 0.2$, $E = 0.5$

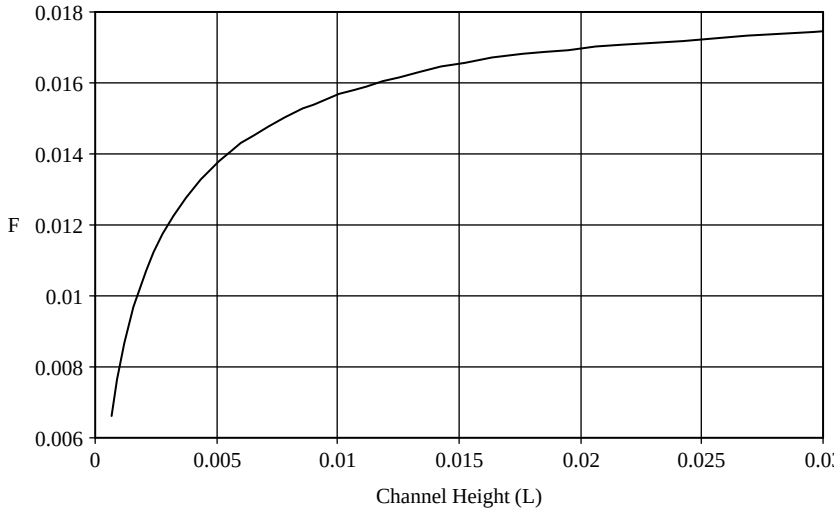

Figure 14.
Variation of flow rate with channel height for radius ratio = 0.7 (Case I) KR = 10, $\delta_i = 0.1$, $\delta_o = 0.2$, $E = 0.5$

However, the dimensional flow rate per unit area for cases (I) and (O) has been calculated and plotted against the corresponding radius ratios in Figure 17. This figure explains the results stated in the previous paragraph as it shows that, whatever the radii maybe, the flow rate per unit area increases as the annulus radius ratio is increased.

Finally, increasing the radius ratio (NR_2) has a direct impact on the total heat absorbed by the fluid as can be seen in Figures 18 and 19 for case (I). Similar trends can be observed in Figure 20 for case (O).

Finally, a reader might be interested in the temperature profiles at different axial locations along the channel as well as the temperature distributions at different cross

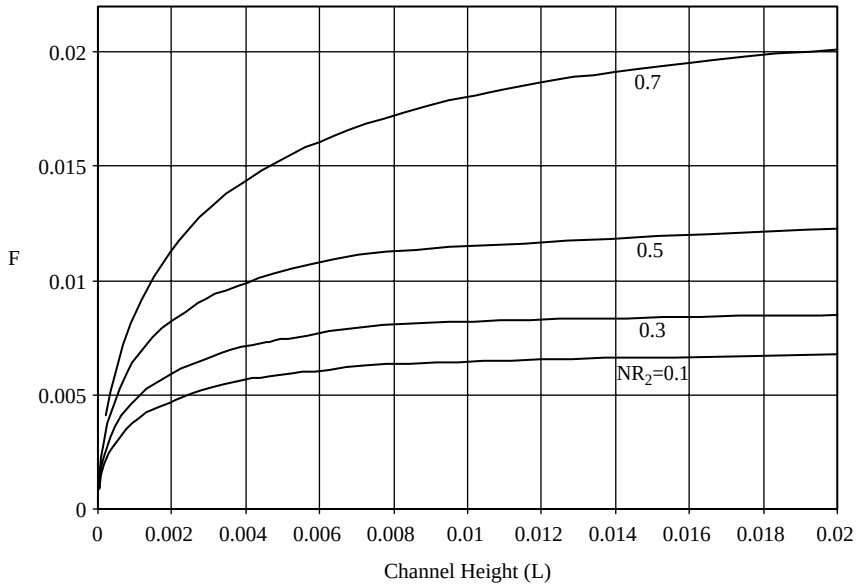

Figure 15.
Variation of flow rate with channel height for different values of radius ratio (Case O) KR $= 10$, $\delta_i = 0.1$, $\delta_o = 0.2$, $E = 0.5$

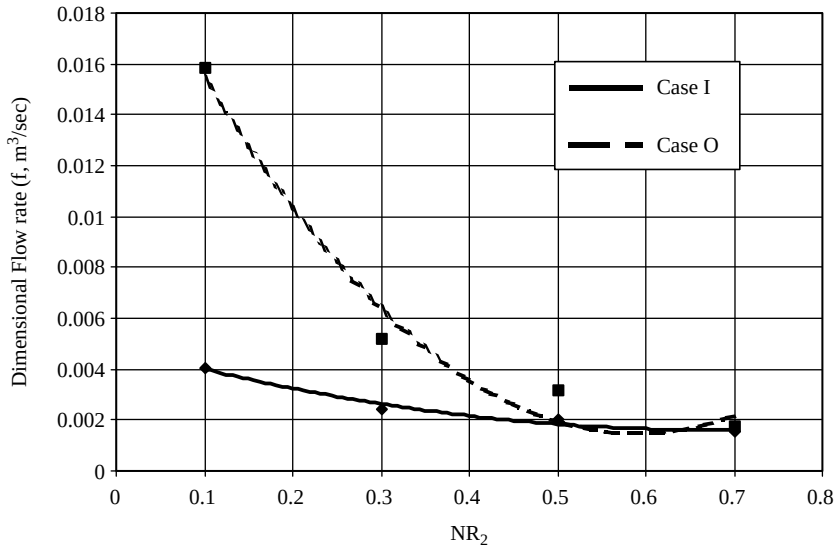

Figure 16.
Dimensional flow rate variation with radius ratio (NR_2) (Cases I and O) KR $= 10$, $\delta_i = 0.1$, $\delta_o = 0.2$, $E = 0.5$

sections of the channel. Such profiles are shown at different axial (vertical) locations for KR $= 1$ in Figures 21 and 22 across the widest ($\psi = 0$) and the narrowest ($\psi = 1$) gaps, respectively. The corresponding profiles for KR $= 10$ are shown in Figures 23 and 24. For KR $= 10$, Figures 23 and 24 show clearly the sudden change in the temperature gradient at the solid-fluid interface.

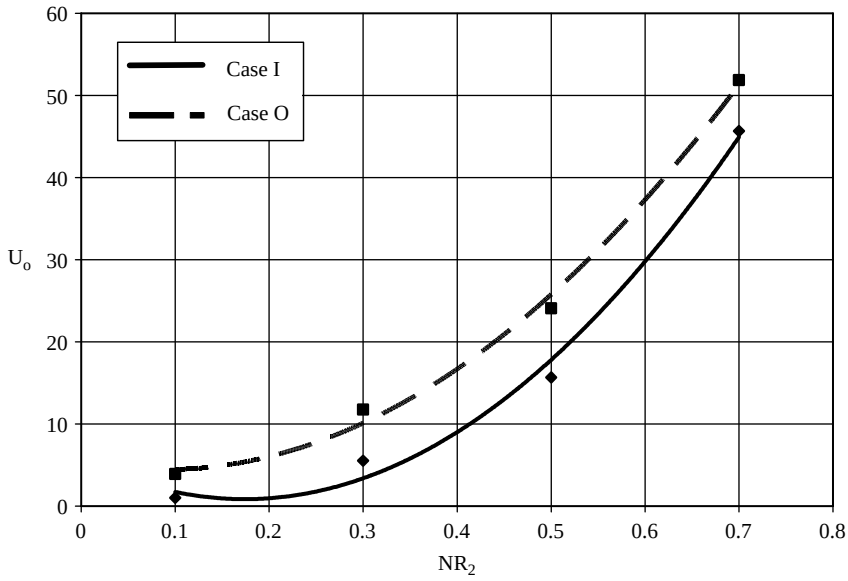

Figure 17.
Dimensional flow rate per unit area varying with radius ratio (NR_2) (Cases I and O) KR $= 10$, $\delta_i = 0.1$, $\delta_o = 0.2$, $E = 0.5$, Axial (vertical)
Location $= 2 \times 10^{-3}$ (for cases I and O)

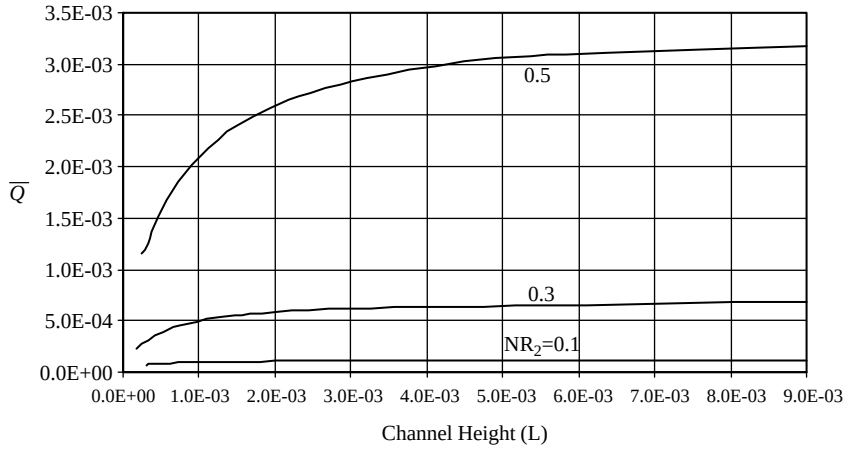

Figure 18.
Total heat absorption versus channel height for different values of radius ratio (Case I)

Conclusions

Conjugate laminar free convection heat transfer in vertical eccentric annuli has been numerically investigated. A finite-difference algorithm has been developed to solve the bipolar model equations. Numerical results have been presented for a fluid of Prandtl number, $Pr = 0.7$ in eccentric annuli. Geometry effects having been investigated by considering fluid annuli having radii ratios $NR_2 = 0.1$ and 0.3, 0.5 and 0.7 and four values of the eccentricity $E = 0.1$, 0.3, 0.5 and 0.7. Moreover, practical ranges of the solid-fluid conductivity ratio (KR) and the wall thicknesses that are commonly available in pipe standards have been investigated.

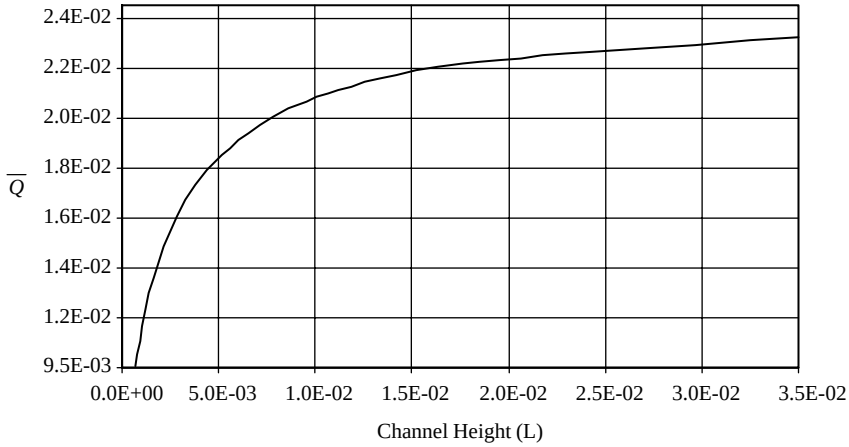

Figure 19.
Total heat absorption versus channel height for radius ratio 0.7 (Case I) KR $= 10$, $\delta_i = 0.1$, $\delta_o = 0.2$, $E = 0.5$

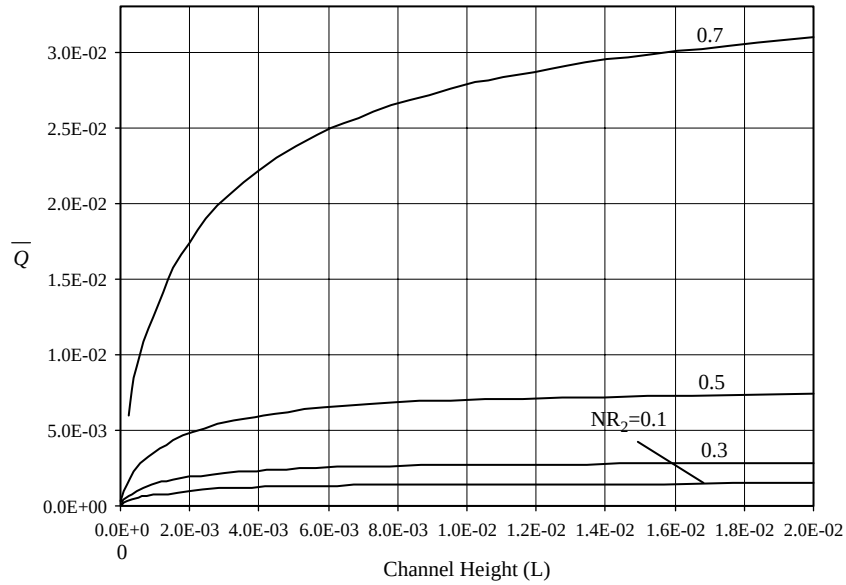

Figure 20.
Total heat absorption versus channel height for different values of radius ratio (Case O)

The results of the present work (conjugate case) have explored distinguished differences from those corresponding to the conventional case (without conjugation). Such results show that, for a given channel height (L), increasing the eccentricity causes an increase in the induced flow rate (F). Similar trend is observed for the total heat absorbed by the fluid ($\bar{Q}$) with the eccentricity. On the other hand, increasing the radius ratio (NR_2) causes the induced flow rate (F) and the total heat absorbed ($\bar{Q}$) to increase. Finally, the obtained results have also shown that heating the outer cylinder wall of the eccentric annulus is more useful for inducing flow (thermosiphons) than heating its inner wall.

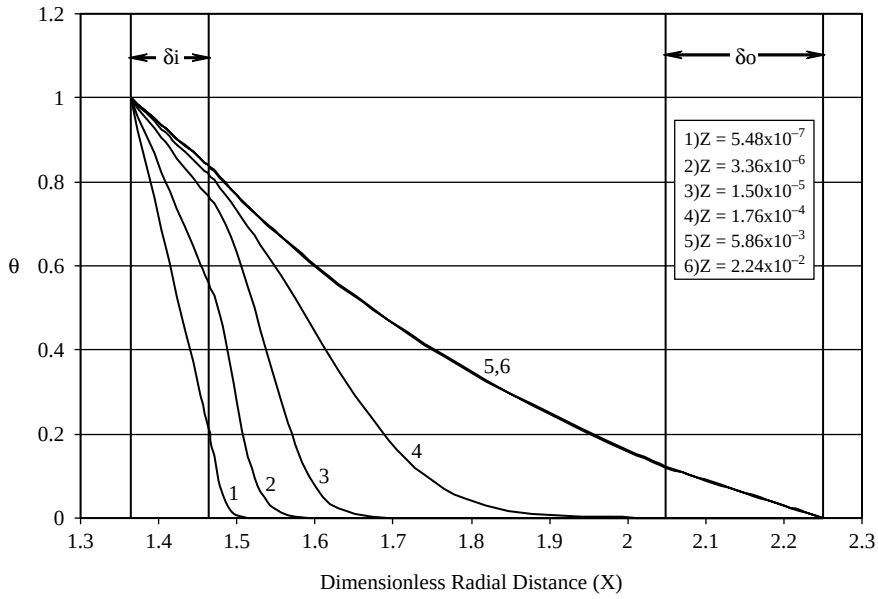

Figure 21.
Temperature profile across the widest gap ($\psi = 0$) at different axial (vertical) locations for case (I), $L = 2.24 \times 10^{-2}$ KR = 1, $\delta_i = 0.1$, $\delta_o = 0.2$, $E = 0.5$, $NR_2 = 0.5$

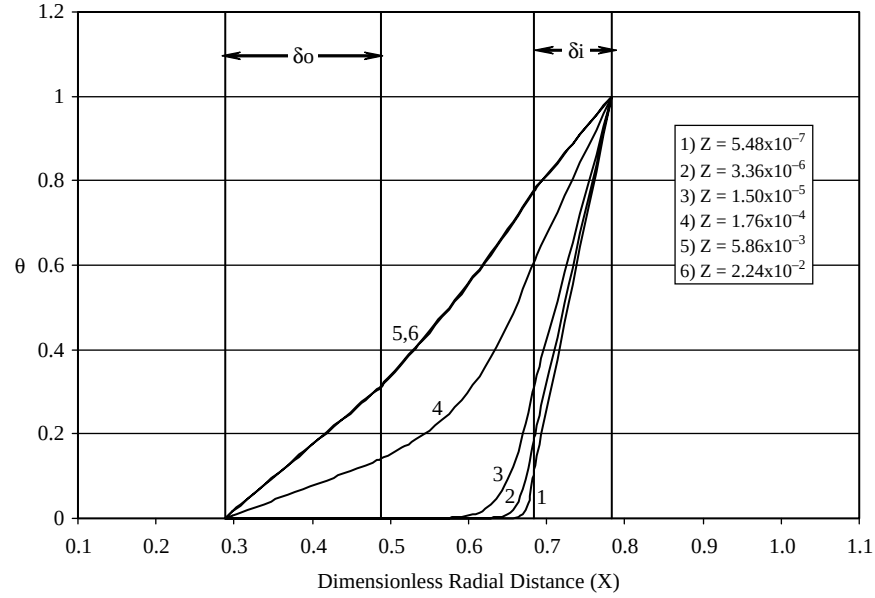

Figure 22.
Temperature profile across the narrowest gap ($\psi = 1$) at different axial (vertical) locations for case (I), $L = 2.24 \times 10^{-2}$ KR = 1, $\delta_i = 0.1$, $\delta_o = 0.2$, $E = 0.5$, $NR_2 = 0.5$

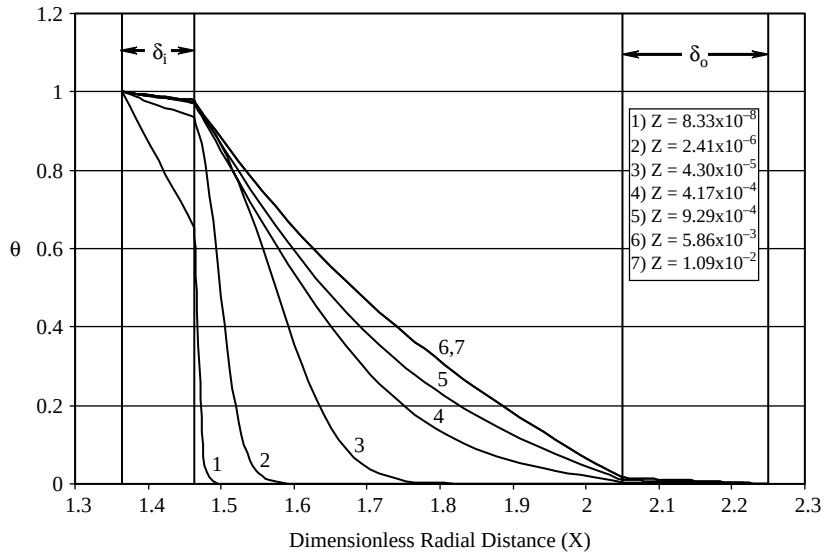

Figure 23.
Temperature profile across the widest gap ($\psi = 0$) at different axial (vertical) locations for case (I), $L = 1.68 \times 10^{-2}$ KR = 10, $\delta_i = 0.1$, $\delta_o = 0.2$, $E = 0.5$, $NR_2 = 0.5$,

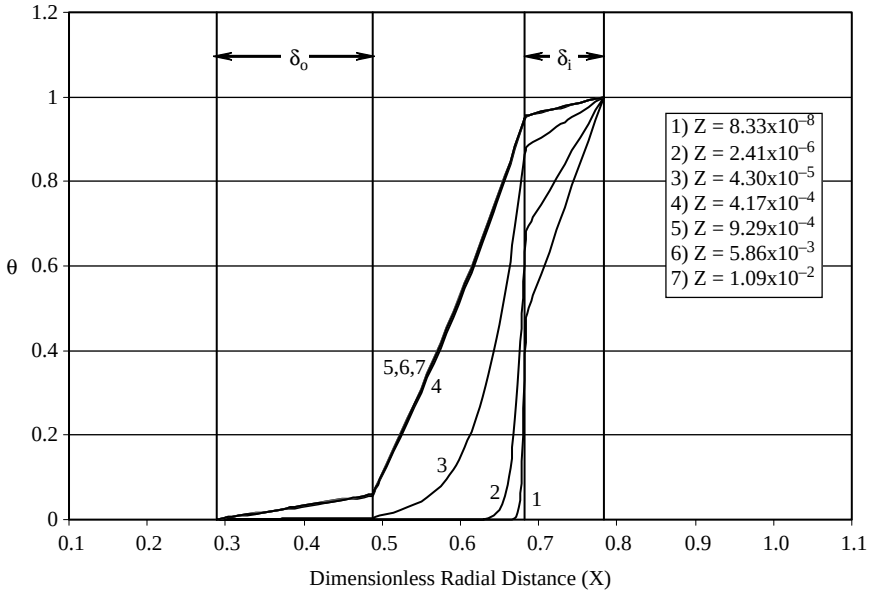

Figure 24.
Temperature profile across the narrowest gap ($\psi = 1$) at different axial (vertical) locations for case (I), $L = 1.68 \times 10^{-2}$ KR = 10, $\delta_i = 0.1$, $\delta_o = 0.2$, $E = 0.5$, $NR_2 = 0.5$

References

Anand, N.K. and Tree, D.R. (1987), "Some studies of the effects of axial conduction in a tube wall on the steady-state laminar convective heat transfer", *Journal of Heat Transfer*, Vol. 109, pp. 1025-8.

Cheng, K.C. and Hwang, G.J. (1968), "Laminar forced convection in eccentric annuli", *A.I. Ch. E. Journal*, Vol. 14 No. 3, pp. 510-2.

Dyler, J.R. and Fowler, J.H. (1966), "The development of natural convection in a partially-heated vertical channel formed by two parallel surfaces", *Mechanical and Chemical Engineering Trans.*, The Institution of Engineers Australia, MC2, Perth, pp. 12-16.

El-Shaarawi, M.A.I. and Haider, S.A. (2001), "Critical conductivity ratio for conjugate heat transfer in eccentric annuli", *International Journal of Numerical Methods for Heat & Fluid Flow*, Vol. 11 No. 2, pp. 255-77.

El-Shaarawi, M.A.I. and Mokheimer, E.M.A. (1998), "Free convection in vertical eccentric annuli with a uniformly heated boundary", *International Journal of Numerical Methods for Heat & Fluid Flow*, Vol. 8 No. 5, pp. 488-503.

El-Shaarawi, M.A.I. and Mokheimer, E.M.A. (1999), "Developing free convection in open ended vertical eccentric annuli with isothermal boundaries", *Journal of Heat Transfer, Transaction ASME*, Vol. 121 No. 1, pp. 63-72.

El-Shaarawi, M.A.I. and Negm, A.A.A. (1999), "Transient combined natural convection-conduction in open-ended vertical concentric annuli", *Heat and Mass Transfer*, Vol. 35, pp. 133-41.

El-Shaarawi, M.A.I., Abualhamayel, H.I. and Mokheimer, E.M.A. (1998), "Developing laminar forced convection in eccentric annuli", *Heat and Mass Transfer*, Vol. 33, pp. 353-62.

El-Shaarawi, M.A.I., Al-Nimr, M.A. and Hader, M.A. (1995), "Transient conjugated heat transfer in concentric annuli", *International Journal of Numerical Methods in Heat & Fluid Flow*, Vol. 5, pp. 459-73.

El-Shaarawi, M.A.I., Mokheimer, E.M.A. and Abulhamayal, H.I. (2001), "Limiting values for free convection induced flow rates in vertical eccentric annuli", *Numerical Heat Transfer, 39A*, Vol. 6, pp. 611-30.

Feldman, E.E., Hornbeck, R.W. and Osterle, J.F. (1982a), "A numerical solution of laminar developing flow in eccentric annular ducts", *International Journal of Heat and Mass Transfer*, Vol. 25 No. 2, pp. 231-41.

Feldman, E.E., Hornbeck, R.W. and Osterle, J.F. (1982b), "A numerical solution of temperature for laminar developing flow in eccentric annular ducts", *International Journal of Heat and Mass Transfer*, Vol. 25 No. 2, pp. 243-53.

Hughes, W.F. and Gaylord, E.W. (1964), *Basic Equations of Engineering Science*, Schaum Outline Series, McGraw-Hill, New York, NY, pp. 150-1.

Jamal, A. (2002), "Conjugate free convection heat transfer in vertical eccentric annuli", MS thesis, Mechanical Engineering Department, King Fahd University of Petroleum and Minerals (KFUPM), Dhahran.

Kim, S.H. and Anand, N.K. (1990), "Effect of wall conduction on free convection between asymmetric heated vertical plates: uniform wall heat flux", *International Journal of Heat and Mass Transfer*, Vol. 33 No. 5, pp. 1013-23.

Kim, S.H., Anand, N.K. and Fletcher, L.S. (1991), "Free convection between series of vertical parallel plates with embedded line heat source", *Journal of Heat Transfer*, Vol. 113, pp. 108-15.

Manglik, R.M. and Fang, P.P. (1995), "Effect of eccentricity and thermal boundary conditions on laminar fully developed flow in annular ducts", *International Journal of Heat and Fluid Flow*, Vol. 16, pp. 298-306.

Mokheimer, E.M.A. (1996), "Heat transfer in eccentric annuli", PhD dissertation, Mechanical Engineering Department, King Fahd University of Petroleum and Minerals (KFUPM), Dhahran.

Redberger, P.J. and Charles, M.E. (1962), "Axial laminar flow in a circular pipe containing a fixed eccentric core", *The Canadian Journal of Chemical Engineering*, Vol. 40, pp. 148-51.

Sakakibara, M., Mori, S. and Tanimoto, A. (1987), "Conjugate heat transfer laminar flow in an annulus", *The Canadian Journal of Chemical Engineering*, Vol. 65, pp. 541-9.

Shah, R.K. and London, A.L. (1978), *Laminar Flow Forced Convection in Ducts*, Academic Press, New York, NY.

Shu, C. and Wu, Y.L. (2002), "Domain-free discretization method for doubly connected domain and its application to simulate natural convection in eccentric annuli", *Computer Methods in Applied Mechanics and Engineering*, Vol. 191 Nos 17/18, pp. 1827-41.

Trombetta, M.L. (1972), "Laminar forced convection in eccentric annuli", *International Journal of Heat and Mass Transfer*, Vol. 14, pp. 1161-72.

Corresponding author
Maged A.I. El-Shaarawi can be contacted at: magedas@kfupm.edu.sa